Study of Heat Capacity Measurement Methods for Small Samples

by

Ronald B. Rogge, B.Sc., Brock

A Thesis

submitted to the department of Physics

in partial fulfillment of the requirements

for the degree of

Master of Science

May 1990

Brock University

St. Catharines, Ontario

Abstract

Methods of measuring specific heats of small samples were studied. Three automated methods were explored, two of which have shown promising results. The adiabatic continuous heating method, has provided smooth well behaved data but further work is presently underway to improve on the results obtained so far. The decay method has been successfully implemented demonstrating reasonable agreement with accepted data for a copper test sample.

Acknowledgments

I would like to thank Dr. F. S. Razavi for taking me on as a graduate student and proposing this research project. Particularly I thank him for his understanding and continuing efforts in supporting my endeavors. I also like to thank Drs. Mitrovic, Plint, Koffyberg and Zaleski for several helpful conversations.

Thanks are also due to the glass blower and members of the electronics department and machine shop for their workmanship and instructional discussions.

Finally I thank my mother, Wilhelmina and girlfriend, Denise, for their encouragement and emotional support. Further I thank Denise for her help in preparing portions of this report.

Table of Contents

List of Tables

List of Figures

Section I

Section II

List of Figures (Continued)

Introduction

Heat Capacity or more precisely the specific heat, the heat capacity per unit mass or per mole, is one of the most fundamental physical properties of a system. Unlike say electrical or magnetic properties, the specific heat can be associated with all states of matter; solid, liquid, gas, ferromagnetic, superfluid et cetera. Nonetheless the inherent difficulty of the measurement has made it a seldomly measured quantity and it is typically left as one of the last measurements made for a system under investigation. On the other hand specific heat is frequently the first experimentally measurable quantity that theorists compute.

The heat capacity is defined as the amount of energy required to raise the temperature of a sample 1K, or mathematically,

$$C_x \equiv \left(\frac{dQ}{dT} \right)_x \qquad (1)$$

where x denotes the physical parameter(s) held constant during the measurement or computation. In other words the heat capacity is a measure of the response of a system in the form of a change in its temperature due to the application of heat energy under certain fixed conditions. Although theoretically x can be any parameter, the usual heat capacities are at constant volume, C_v, and at constant pressure, C_p. In theory the heat capacity at constant volume is readily calculated from either the entropy, S, or the free energy, F, using the relations,

$$C_v = T \, (\partial S/\partial T)_v \qquad (2)$$

and

$$C_v = -T \left(\partial^2 F/\partial T^2\right)_v \qquad (3)$$

respectively. For solids, one is restricted to measuring C_p. The difference, $C_p - C_v$, for solids is typically less than 5% [13].

It is unfortunate that heat capacity measurements are frequently delayed or left out, as a great deal can be learned from its measurement. Specific heat is a direct result of the net effect of microscopic phenomena and thus, although the specific heat is a so called bulk property, information about such microscopic properties as the density of states can be extracted from its measurement. Also the so called specific heat anomalies give information about the nature of a phase transition and the system's order. For example if during some temperature interval the sample's temperature remains fixed the energy going into the sample must therefore be used for some other process such as a structural change. This sort of behaviour is typical of a first order phase transition and leads to a peak in the specific heat as a function of temperature. Also looking at equation (2) we see that if the system suddenly becomes more ordered there is a jump or discontinuity in the specific heat due to the sudden change in its entropy, this is typical of a second order phase transition.

Phase transitions is the raison d'être for our interest in specific heats. The need to be able to measure small samples is

simply a result of the size of samples available in modern research. The desire for high purity samples or single crystals frequently limit the size of the sample to much less than 1g. This leads to a small heat capacity affecting the accuracy of the measurement as the sample heat capacity becomes comparable to addenda which must be subtracted from the experimental data.

In general the thermodynamic response of a typical apparatus used to measure heat capacities, can be described by the so called diffusion equation,

$$P + dQ/dT = C\ dT/dt \qquad (4)$$

where P is the power supplied to the sample, dQ/dT is the rate of heat exchanged with the system's environment and C dT/dt represents the portion of the power which goes to heating the sample. It is clear that if dQ/dT = 0 the heat capacity is readily obtained by simply applying a known amount of power and measuring the resulting change in temperature. However in practice this is simply not possible and all the various methods of measuring heat capacity differ only in how they deal with the exchange with the environment.

In all three methods were investigated in this research; The modified heat step method of section II is based on the work of DePuydt an Dahlberg [1]. Here the thermal conductance of the thermal link to the environment is estimated by examining the system in the steady state, characterised by dT/dt = 0. The conductance, K, is then defined as $-dQ/dt = K\ (T-T_B)$, where T_B is

the environment temperature. Then the diffusion equation gives K = P / ($T-T_B$) in the steady state. This information is used to estimate the conductance in the dynamic situation described by the diffusion equation in order to compute the heat capacity. This method proved unsuccessful in that the heat capacities obtained showed a high degree of scatter.

The continuous heating method based on the work of Junod [2] is discussed in section III. Here the exchange with the environment is handled by considering the system under two different conditions in which the exchange is considered to be the same. That is the system is measured with and without power supplied to the sample so that the diffusion equation leads to two equations with two unknowns, C and dQ/dt, which can then be solved. This method has provided favourable results for the so called pseudo heat capacity. However further experiments are underway to improve some aspects of the method.

Section IV details the investigation of the decay method based on the works of Bachmann et al [3] and Lawless et al [10]. Here the actual determination of the thermal conductance is circumvented and instead the power required to raise the sample to some temperature above the environment is measured as a function of temperature. This information is then used to compute the heat capacity as the sample temperature decays to the environment temperature, from some elevated temperature, once the power supplied to the sample is shut off. This method was the most

successful of the three, providing well behaved and reproducible results that seem in good agreement with accepted data for Copper.

Another objective of this research was that the heat capacity measurement system be fully automated under computer control and capable of measuring heat capacities in the full temperature range of ~5 - 300K. This range is consistent with other experiments performed in Dr. Razavi's lab and provides a convenient reference at room temperature. The last two methods cannot cover this full range independently but complement each other with a common range at about 40K, i.e., the continuous heating method is applicable from 40K up to 300K and the decay method works well below 40K.

Section I details the two basic designs for the apparatus, thermal electrical and mechanical aspects are discussed. Several computer programs were written in the progress of this research and were designed to make the heat capacity measurement system a turn-key system. These are not discussed in this volume, along with some other peripheral works, that are discussed in a supplemental volume entitled, Supplement to a Study of Heat Capacity Measurement Systems.

Section I: Basic Apparatus Designs

In all, three different techniques for measuring heat capacity were explored (see references 1-3). However certain aspects of the apparatus remain consistent to one of two basic designs. This section then describes the basic elements of the two designs.

I.1 Cryostat Considerations of Design 1

The first apparatus (fig. I.1) was designed for installation into the stainless steel cryostat from Cryo Industries of America Incorporated model 8CC LHe [4]. The inner or sample chamber can be evacuated to reduce thermal exchange via gas. At the top of the chamber, connectors in the head provide electrical contact to outside the cryostat. Also attached to this head is a long stainless steel rod which can be moved vertically within the chamber and is used to support the sample. The bottom portion of the chamber is copper for good thermal contact between the liquid bath and lower sample space which houses a mylar window (this cryostat is primarily designed for use with Mössbauer systems).

At the bottom of the stainless steel rod in the inner chamber is the sample cell (fig. I.2). The first segment of the cell is a teflon rod which is threaded at the top and bottom and provides a low thermal conductivity extension to the stainless steel support rod. This helps further isolate the rest of the cell from the outside environment. Next in the cell is a copper cup which faces up. The side of the cup is cut vertically to form fingers

Figure I.1, First Cryostat

A: Electrical connectors, B: Head unit,
C: stainless portion of sample chamber wall,
D: copper cup with tension fingers,
E: copper portion of chamber wall,
F: stainless steel rod, G: inner coolant chamber,
H: outer coolant chamber, I: sample chamber.

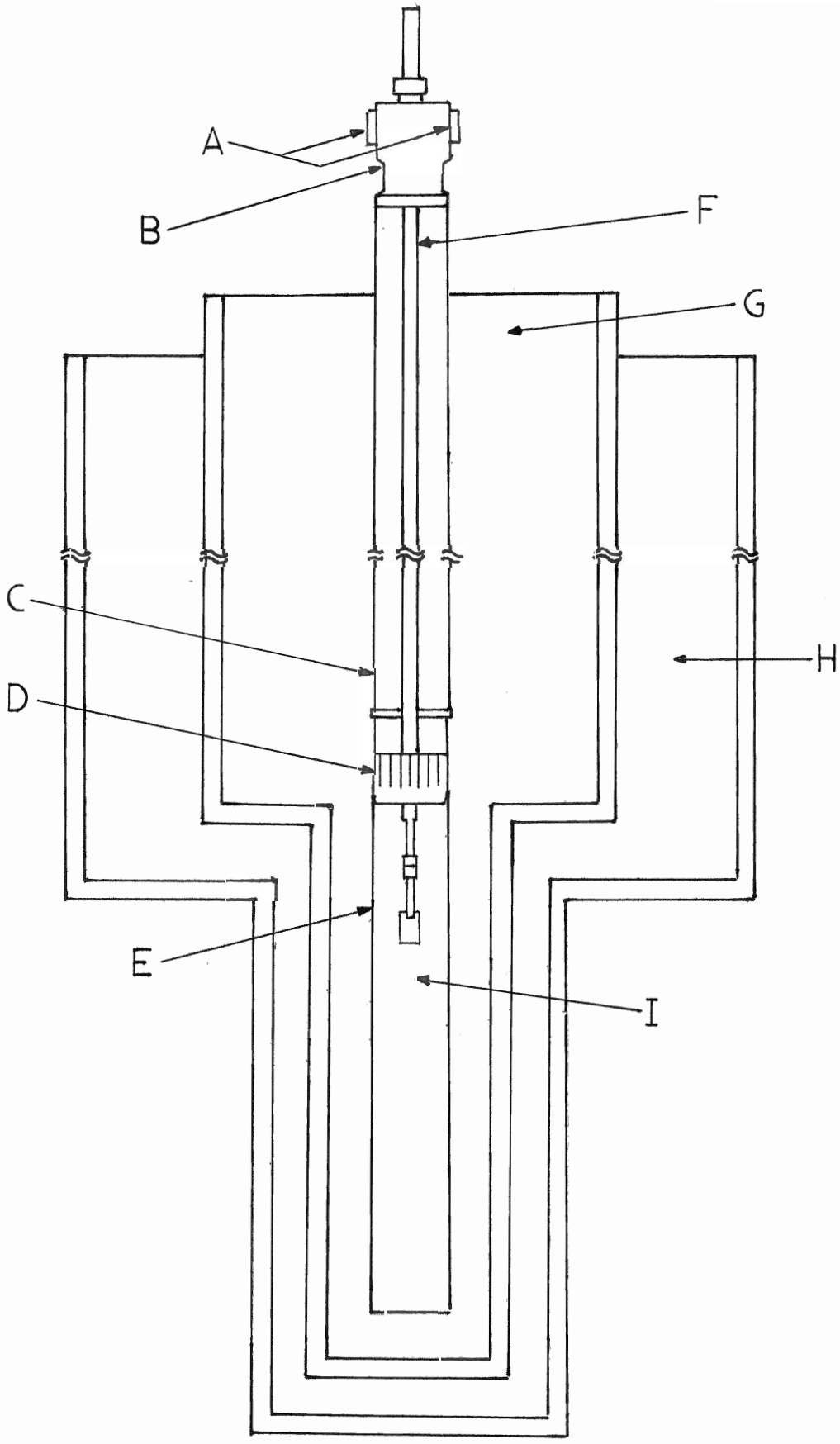

Figure I.1

which are bent outward to maintain good thermal contact with the copper segment of the chamber wall which is surrounded by a liquid bath in the middle chamber. A double ended screw passes through the base of the cup to secure to the teflon rod above and the next copper section of the cell below. The base of the cup is thick for high thermal conduction and has four small holes drilled through it to allow wires to pass through to the lower part of the cell. The next component is a copper mass with a resistance wire heater doubly wrapped, so that the total magnetic field due to the heater is zero. Heater power is controlled by the Scientific Instruments Series 5500 temperature controller [5] such that the copper mass's temperature remains constant at a specified set point. The temperature of this copper mass is then taken to be the so called bath temperature. The liquid bath shall always be explicitly named as such, to distinguish it from the copper bath.

Mounted below the heated copper mass is a single piece of solid delrin machined into a cylindrical T shape. This rod provides rigid support to the sample mount as well as thermal isolation from the copper bath. The rigid support is useful if any measurements in a magnetic field are desired. At the bottom of the delrin rod a narrow V grove is cut vertically so that the sample mount can be firmly inserted.

The sample mount (figure I.3) consists of a thin (60 ± 7 μm) OFHC (oxygen free, high conductivity) copper sheet measuring (10.0 X

Figure I.2, Sample Mount Assembly

A: stainless steel rod, B: teflon rod,
C: copper cup with tension fingers for thermal contact to sample chamber wall,
D: bath heater wire, E: delrin sample support 'T' rod,
F: OFHC copper sample mount sheet,
G: copper sample chamber wall.

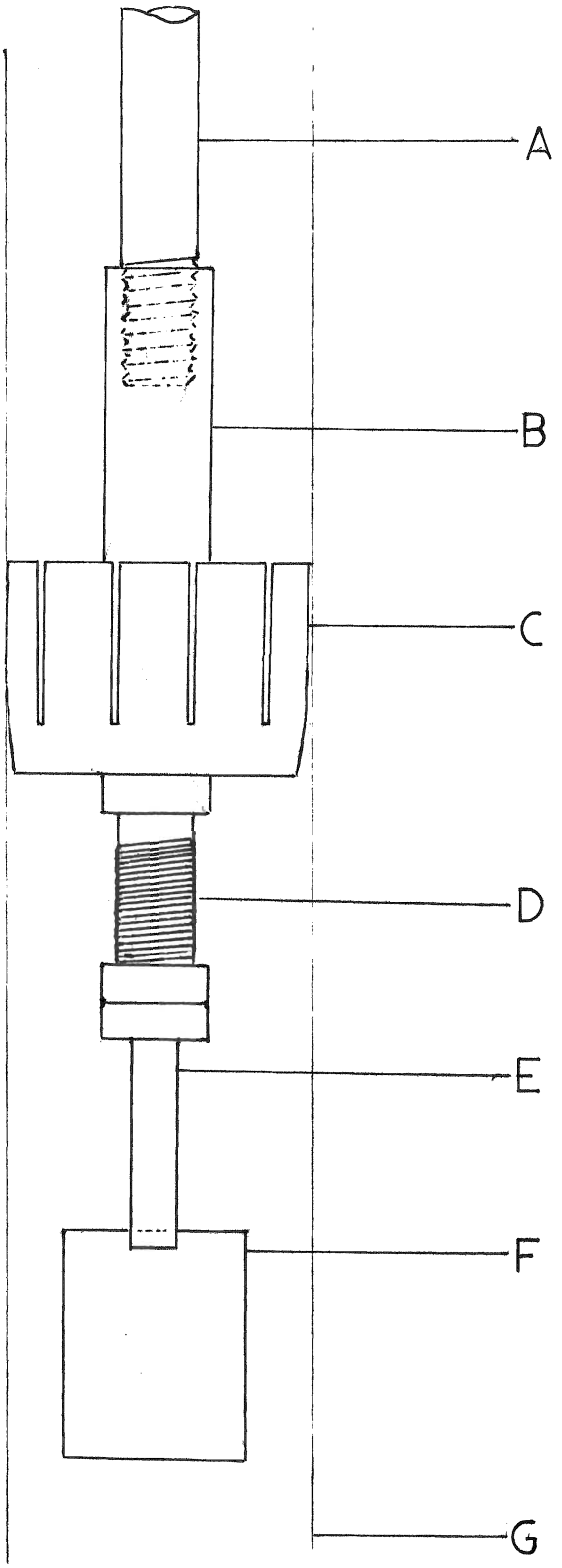

Figure I.2

10.0) ± 0.5 mm and mass 47.17 ± 0.01 mg. A strain gauge, used to provide Joule heat, is mounted onto the sheet with thinned General Electric (GE) 7031 varnish. To achieve the best thermal contact between the strain gauge and sheet, pressure is maintained over the strain gauge surface until the varnish is dry. In the same fashion, a sample is mounted on top of the strain gauge and finally the temperature sensor is mounted on the sample.

A fashioned electrical connector is mounted on the stainless steel rod for all non-thermocouple wires. In this way the wires running along the rod can be left undisturbed. The wires below the connector can be quickly soldered to Y shaped pins. This arrangement maintains good electrical contact from 4.2 - 300K.

The wires running from the connector to the sample cell are then wrapped at several locations (fig. I.4) on the cell to thermalize the wires. This thermalization is necessary to reach low temperatures, otherwise heat from the outside environment flows down the wires raising the cell temperature well above the liquid bath temperature.

The wires are wrapped on four sections. The first is around the teflon rod to prevent tension in the wires at the connectors and to keep them from being pinched between the cup and the chamber wall when the cell is removed from the chamber. This wrap is not really intended to thermalize the wires, but nonetheless should

Figure I.3, Detailed Sample Mount

A: copper bath, B: support screws,
C: delrin sample support rod,
D: differential thermocouple,
E: OFHC copper sample mount sheet,
F: sample thermometer, G: sample,
H: strain gauge sample heater,
I: cigarette paper and varnish.

Figure I.4, Thermalization Points

A: electrical connector,
B: wires wrapped on teflon rod,
C: brass anchoring pins,
D: wrap point below heater,
E: wrapped for support,
F: long hanging wires for small conductance.

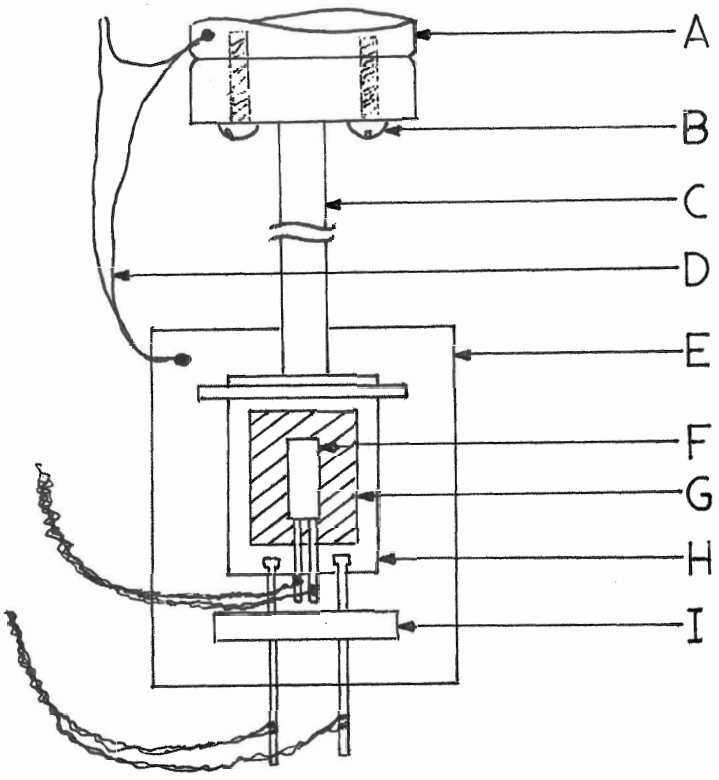

Figure I.3

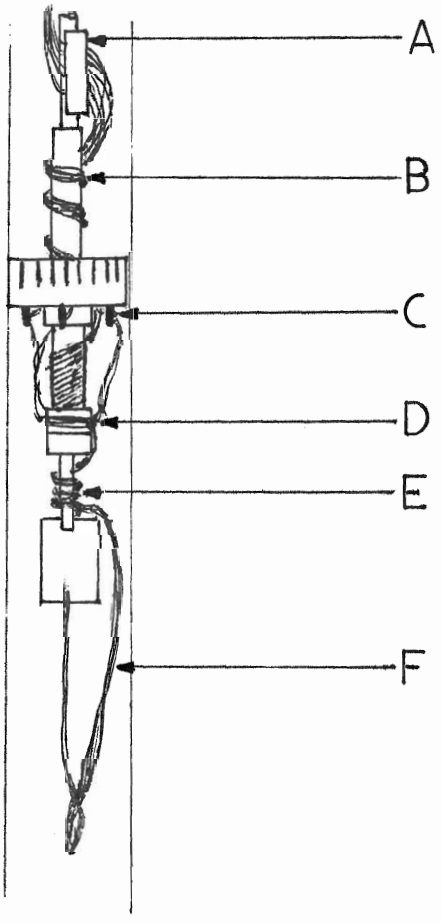

Figure I.4

bring the wires much closer to the liquid bath temperature than the temperature of the outside environment. The wires are also wrapped a few times around several brass pins on the underside of the copper cup. Then the wires are wrapped several times on the copper mass just below the heater to thermalize the wires to the temperature of the copper mass. A portion of the remaining length of the wires, ~15 cm, are wrapped in a spiraling fashion down the delrin rod towards the sample mount. This wrap prevents the wires from making thermal contact with the chamber wall. The final 5-7 cm hangs down past the sample mount and back up to the sample mount. This grouping of wires is sufficiently stiff that by tying them to the delrin rod and bending the wires, contact to the chamber wall can be prevented.

I.2 Acquisition Equipment of Design 1

Figure I.5 shows the block diagram diagram of the data acquisition system. There are five major components of the system. Firstly an IBM XT compatible computer is the central control unit. All control with the exception of maintaining bath temperature is executed by programs written in GW Basic (discussed in appendices [12]). Installed in the computer are two interface boards. The first provides a digital to analog converter (DAC) and a analog to digital converter (ADC). This board was produced here and is discussed in detail in appendix A [12a]. For design one, its sole purpose is to provide precise control of the power supplied to the strain gauge heater (resolution of better than 0.3 nW). The second is an IEEE-488

interface produced by Scientific Solutions [6] which is designed to conform to the standards given by Hewelt Packard the designers of the IEEE interface. This interface is used to communicate with the temperature controller and a multichannel digital multimeter. The temperature controller [5] uses a Si diode temperature sensor (calibrated from 1.5 to 350K by Scientific Instruments) and a digital PID (proportional, integral and derivative) control scheme to attain and maintain a set point temperature sent by the computer via the IEEE.

The other IEEE device is a Prema integrating multimeter with a scanner option for multiple inputs [7]. The Prema meter is responsible for many of the measurements of this system. Four channels are used, the first, channel 0 measures the voltage across a pair of thermocouples to verify that the copper bath and sample are at the same temperature within a small error of approximately ±5μV (maximum temperature error of ~0.3K). Actual temperature error is likely less than this since part of this voltage error is due to small zero offset error in the Prema meter. Channel 1 is used to measure the signal from the sensor used to measure sample temperature. Various sensors were considered such as Alan Bradely, iron gold thermocouple, copper constantan thermocouple, carbon glass and Si diode.

To precisely measure the power delivered by the strain gauge, the potential drops across the strain gauge and a calibration resister are measured on channels 8 and 9. The calibration

Figure I.5, Acquisition Block Diagram

B: sample thermometer voltage,
C: thermocouple voltage,
D: calibration resistor voltage,
E: strain gauge voltage,
F: bath thermometer voltage,
G: bath heater,
H: sample heater (strain gauge).

Figure I.6, Electrical Connections

D: DAC and power amp power source for strain gauge,
R: calibration resistor, H: strain gauge heater,
S:constant current supply,
T: temperature sensor,
BT: bath temperature sensor (Si diode),
BH: bath heater.

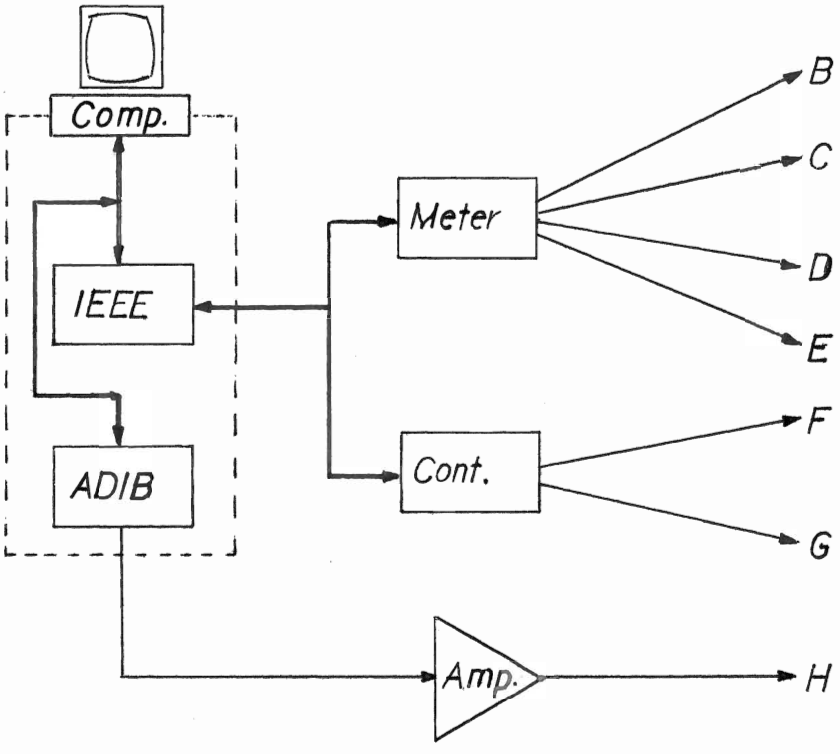

Figure I.5

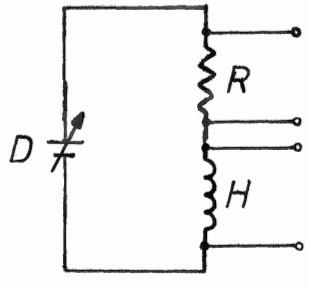

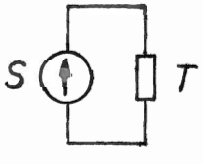

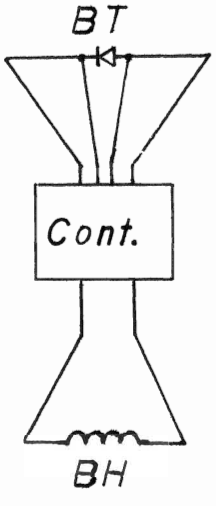

Figure I.6

resistor has a low temperature coefficient, 1ppm/C^{o} and is enclosed in a insulated metal box at room temperature. The resistance was measured by the four probe technique and found to be 99.75 ± 0.01 Ω. The resistor was connected in series with the strain gauge to indirectly measure the current supplied to the strain gauge.

Figure I.6 details the electrical connections to the elements of the sample cell. With the exception of thermocouples all readings are performed using the four probe technique with constant current supplies. Current directions are not switched since it was feared that the modulated currents would result in small undesirable temperature fluctuations and current switching is inappropriate for diode sensors.

I.3 Cryostat Considerations of Design 2

This new design was required because it was found that thermal radiation was a problem in the first design. Efforts were made to provide a radiation shield with the first design but the available space was too confining and shielding could not be provided without the occurrence of thermal shorts.

The second apparatus was designed for use in a glass cryostat made by the glass blower here at Brock. The sample mount is basically the same as for design 1 except that the thermometer is mounted beside the sample such that it is simultaneously in thermal contact with the sample and mount.

This design differs from the previous design primarily in the sample chamber construction (fig. I.7). Here a large copper and brass re-sealable cylinder is attached to the end of a long stainless steel tube. Stainless steel has been frequently used here since it is a hard metal with a much lower thermal conductivity than copper. At the top of the tube, a copper and aluminum head provides passage to the outside environment.

The copper cup of the head unit (fig. I.8) provides a copper tube for attaching a vacuum system for evacuation of the sample chamber. Another small tube provides a pass-through for thermocouple wires used with a liquid bath as a reference temperature. This tube is presently sealed with some tin solder since no thermocouple is in use. The top of the head is a thick (~2cm) aluminum disk into which a standard male 25 pin D-shell connector was attached to provide electrical contact between the sample chamber and the outside (fig. I.8). To ensure a good vacuum seal, long copper posts were soldered to the back of the connector pins, then the deep hole behind the connector was filled with several layers of aluminum epoxy. A rubber O-ring is used to seal the head when the aluminum top is attached to the copper cup. This construction has proven to be very effective, as vacuums down to $\sim 10^{-6}$ Torr have been achieved.

The sample chamber, attached to the bottom of the stainless steel tube, consists of a copper and brass canister which is comprised

Figure I.7, Second Cryostat

A: calorimeter head, B: top sealing plate,
C: inner glass chamber for liquid coolant,
D: stainless steel rod, E: copper fingers,
F: brass flanges, G: copper outer casing,
H: liquid coolant.

Figure I.8, Calorimeter Head

A: electrical connector,
B: thermocouple pass through tube,
C: copper cup, D: aluminum epoxy,
F: aluminum cap, G: evacuation tube,
H: stainless steel rod, I: grounding screw.

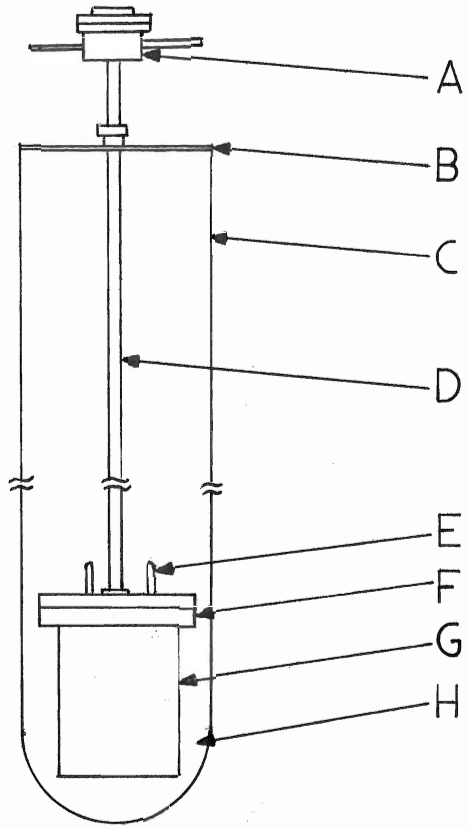

Figure I.7

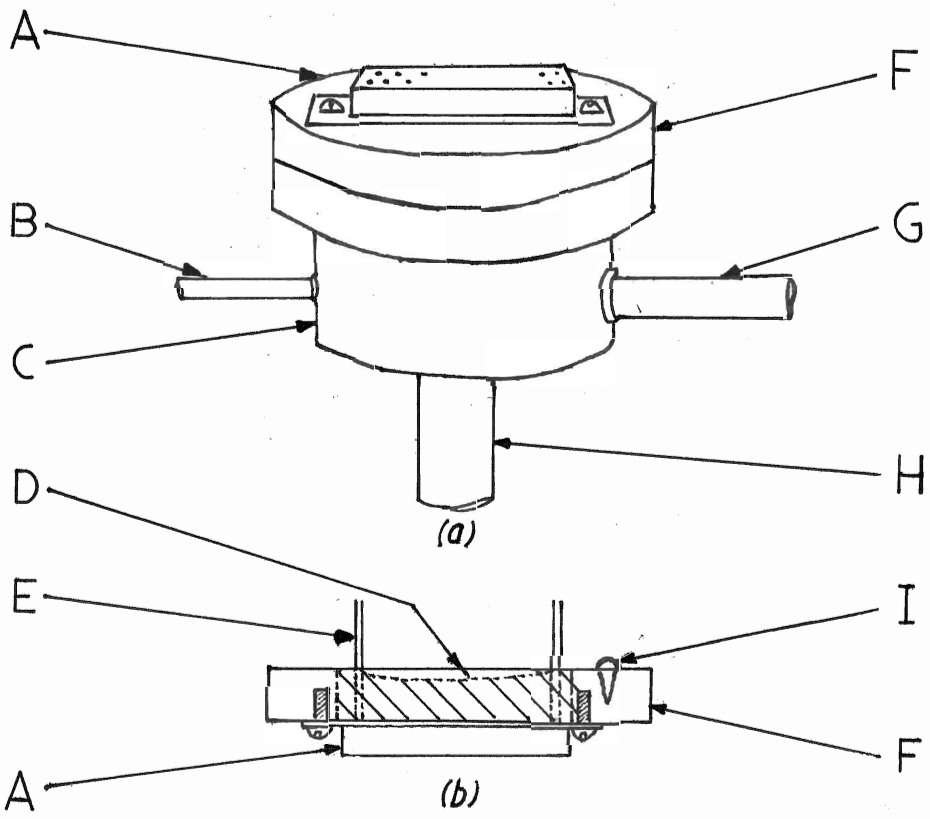

Figure I.8

of three components (fig. I.9(a)). The outer casing is a copper can with a large brass flange at the top used to secure the can to the rest of the cell. Crushed indium provides a vacuum tight seal suitable for low temperatures (ie. liquid He). The second component is the radiation shield, and is simply a copper can of smaller diameter than the casing and concentric to it. A doubly wound wire heater provides Joule heat to this cylinder. The last portion of the cell provides support and electrical connection to the outside via wires running up the inside of the stainless steel tube to the connector in the head. The top of this portion is a brass disk machined to accept the outer canister. A hole at the centre of the disk allows the stainless steel tube to pass through to the inside of the cell providing a passage to the top of the chamber for wiring and a means to evacuate the cell. Two solid copper rods also pass through the brass flange to provide excellent thermal contact with the liquid bath which surrounds the cell. One of the fingers continues lower into the cell and has a double wound heater for the second stage heating as in design one. The temperature of the large copper mass below the heater is the so called bath temperature.

Attached to the copper rod is a second small diameter disk with flat fingers like that on the cup of the first design, to provide thermal contact with the radiation shield when it is slid into place over this disk. The heater on the shield is intended to ensure that the shield temperature is uniform and provide support to the bath heater since the combination of the disk and shield

form a large copper mass compared to that in design one.

Next, hanging from nylon threads, is the sample mount which, with the exception of the thermometer placement is identical to that used in design one. However in this design the wires are coiled and suspended in the vacuum space to provide better isolation from the copper bath. The wires are then soldered to a connection plate which is attached to a long nylon screw (~2.5cm). The connection plate provides a convenient connection point and allows fine wires (no. 50 copper) to be used for electrical contact to the temperature sensor. Using fine wires improves thermal isolation and more importantly reduces tension in the wires which had been found to occasionally pull the thermometer from the mount.

Again the wires must be properly thermalized in order to cool the system and obtain accurate measurements. Achieved in this design by wrapping the wires entering the cell several times around the copper rods and two brass screws in the brass top of the cell. The wires then are soldered to a connector like that in design one. Wires leaving this connector are then thermalized to the copper bath temperature except the four connected to the bath and shield heaters. Figure I.9(b) shows the thermalization points and electrical connections.

In both designs various wires are used. The wires carrying power to the heaters are all no. 30 copper wire. However for the

strain gauge, the wire below the connector at the top of the cell, are phosphor bronze no. 32 wires. Also as discussed earlier no. 50 copper wire is used near the sample mount to reduce tension (for thermometer only). All other wires are no. 36 phosphor bronze quad ribbon wire from Lakeshore Cryogenics.

I.4 Data Acquisition Equipment of Design 2

Figure I.10 is a block diagram of the acquisition system. Again the computer is the central control unit with programs written in either Quick Basic or GW Basic, guiding control. New in this design is the Lakeshore DRC-91C temperature controller [8]. This controller returns two temperature readings, the bath temperature controlled by this unit and the sample temperature. The controller is equipped with a precision option, which is used with a precision calibrated Si diode from Lakeshore, allowing measurements with a resolution down to 3mK. The Scientific Instruments Series 5500 controller is used again, but here to control the shield temperature. Again communication is provided by the IEEE interface.

The DAC is again used to control power supplied to the sample, but here the ADC on this board is also used. The board also has an analog multiplexer used to select one of eight channels to be read by the ADC. Channels 0 and 1 are used as in design one to measure actual power dissipated by the strain gauge.

The design described here is the most used configuration. As

Figure I.9, Sample Cell

(a)
A: stainless steel tube,
B: thermal contact copper fingers,
C: crushed Indium seal, D: brass flange,
E: electrical connector, F: bath heater,
G:bath thermometer, H: copper bath plate,
I: nylon support strings, J: sample mount,
K: outer casing, L: radiation shield,
M: shield thermometer.

(b)
A: brass anchoring screws,
B: thermal wrap at bath temperature,
C: primary thermal link,
D: hanging coiled electrical wires.

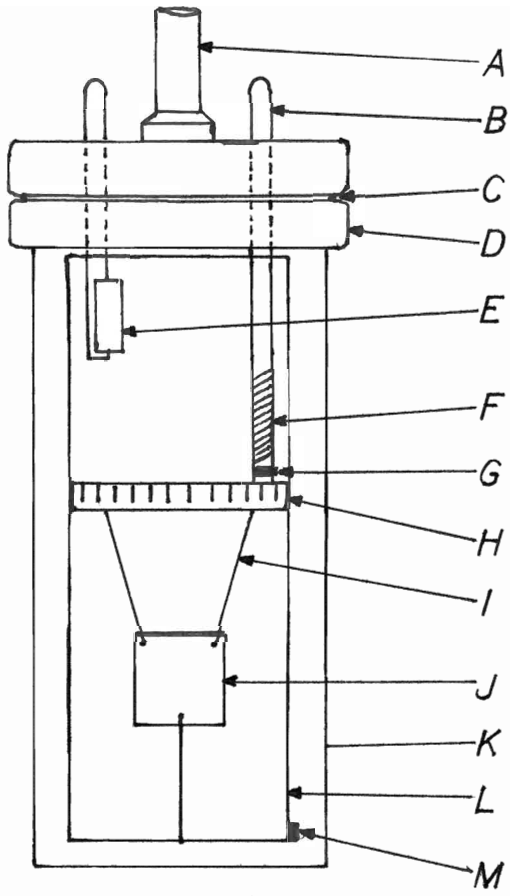

(a)

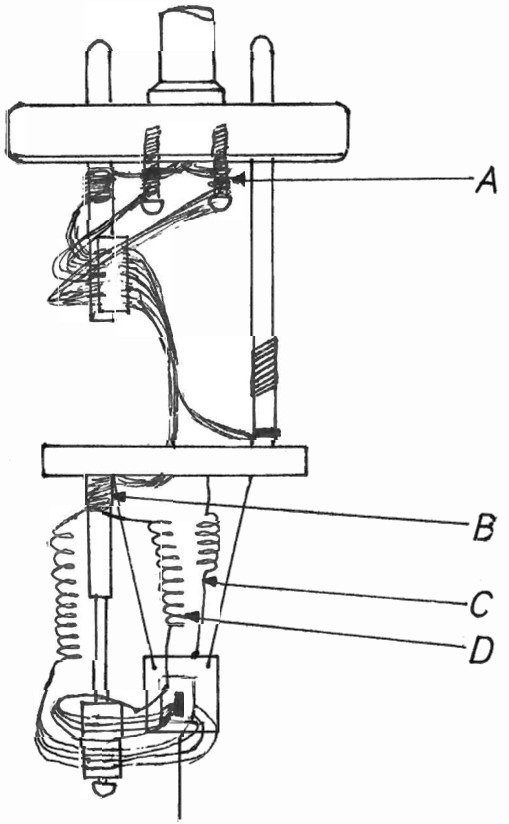

(b)

Figure I.9

Figure I.10, Block Diagram

A: calibration resistor, B: strain gauge,
C: bath heater, D: bath thermometer,
E: sample thermometer,
F: shield heater, G: shield thermometer.

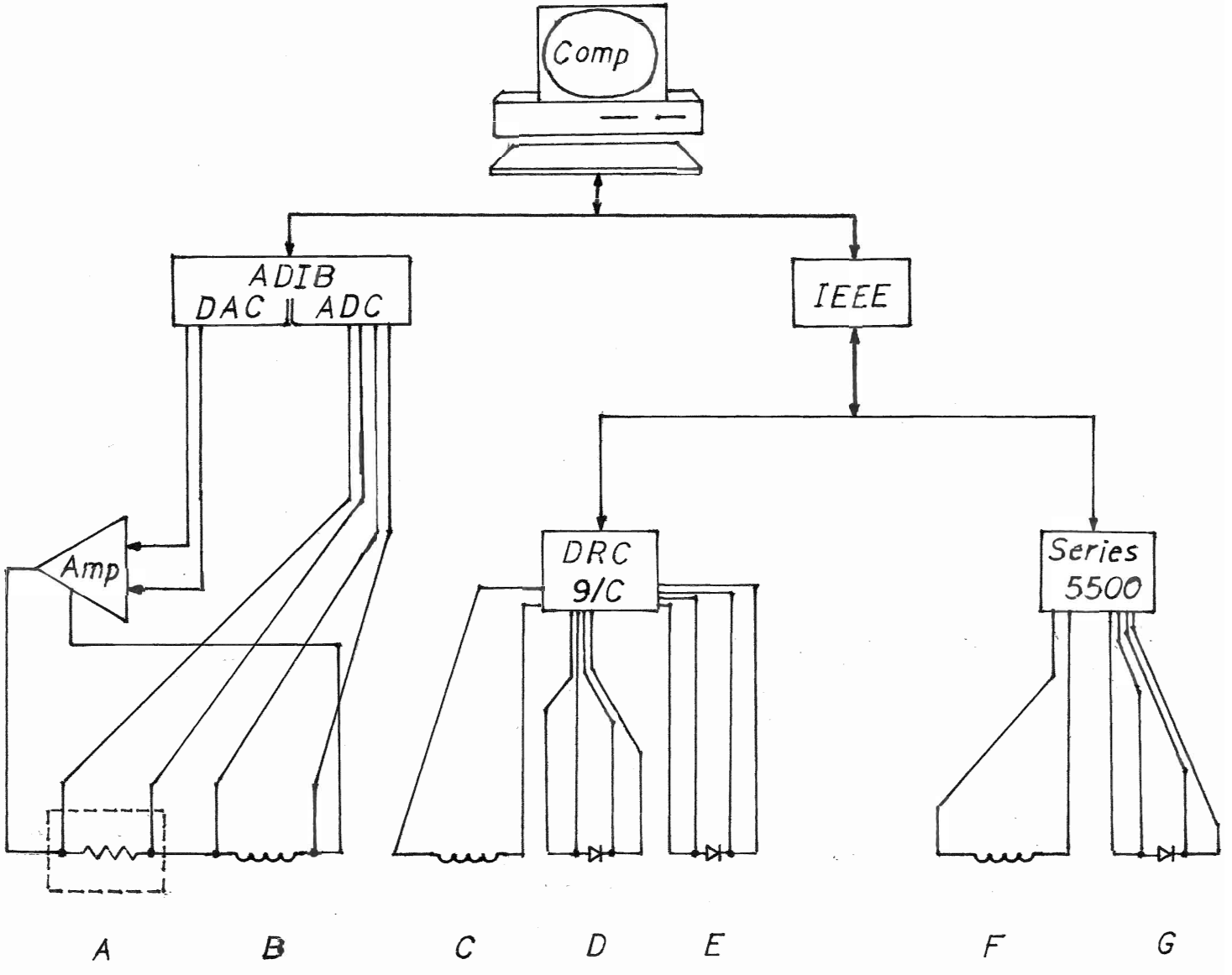

Figure I.10

usual the system underwent many changes during development. Most importantly the final apparatus is a little different than given here. These important changes are described near the end of section IV. Any other important differences are likewise discussed in the appropriate sections.

Section II: The Modified Heat Step

II.1. Theory of Measurement

The first experimental design was modeled in part, after the method of DePuydt and Dahlberg [1]. The basis of this method stems from an analysis of the thermodynamic equation of state of a system consisting of a sample, S (in this report, sample shall refer to simplified case of figure II.1) in thermal contact with some large reservoir, or bath, B, of fixed temperature T_B. Some of the power, P, supplied to S goes to heating the sample and the remaining portion is lost via the link of effective thermal conductance, K, to the bath, thus we have,

$$P = C\,(dT/dt) + K\,(T - T_B), \qquad \text{(II.1)}$$

where S has total heat capacity C and is at temperature T. This equation is also referred to as the diffusion equation. The temperatures and time can be directly measured and the power set externally. Therefore C can be calculated if we know the conductance, K.

If power is supplied in a sufficiently small amount, the rise in sample temperature is small (< 0.1 K) and we can assume that C is reasonably constant during the heating step. Rearranging equation (II.1) as,

$$dT/dt = P/C - (K/C)(T-T_B), \qquad \text{(II.2)}$$

and solving for C we obtain the integral equation,

$$C = \frac{Pt - {}_0\int^t K[T(t')]\,(T(t')- T_B)\,dt'}{T(t) - T(0)} . \qquad \text{(II.3)}$$

where K is taken to be a function of T which is itself a function

of time, t, thus denoted K[T(t)]. Now, looking back to the diffusion equation (II.1), we see that at the end of a heating step (figure II.2) the sample is in some new thermodynamic equilibrium and steady state temperature T, then dT/dt = 0 and (II.1) reduces to

$$P = K(T - T_B). \qquad (II.4)$$

The conductance can then be calculated at this temperature by

$$K = P / (T - T_B). \qquad (II.5)$$

Therefore K can be indirectly measured at the end of each such heating step. If the sample is heated by successive heating steps both the initial and final values of K are known for each step except the first. Then rather than using an average value for that step, K can be estimated by a linear function of T for a small temperature step, that is for some heating step,

$$K[T(t)] = K_o + \frac{K - K_o}{T - T_o}(T(t) - T_o) \qquad (II.6)$$

where K_o is the conductance at the beginning of the present step (ie. $K_o \equiv K[T(0)]$ of this step = $K[T(t)]$ of the previous step) and K is the conductance at the end of the step, ie. $K[T(t)]$. Similarly T and T_o are the steady state temperatures of the present and previous steps respectively and T(t) is the sample temperature at the time t during the present step.

In summary the thermodynamic response of the apparatus is given by the diffusion equation (II.1), which when analyzed shows that the observables are bath temperature, sample temperature, time and power supplied to sample. The effective thermal conductance

Figure II.1, Simplified Model

B: large thermal reservoir at temperature T_B,
K: effective thermal conductance,
S: sample, P: power supplied to sample.

Figure II.2, Ideal Heating Steps

Shows ideal heating of sample in thermal contact with a bath at temperature B. The end of step 0 provides a starting point the experiment. The first data is taken on step 1.

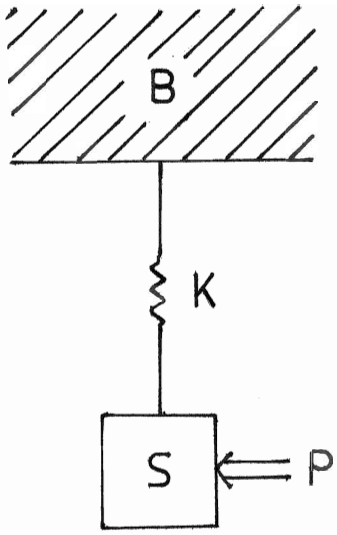

Figure II.1

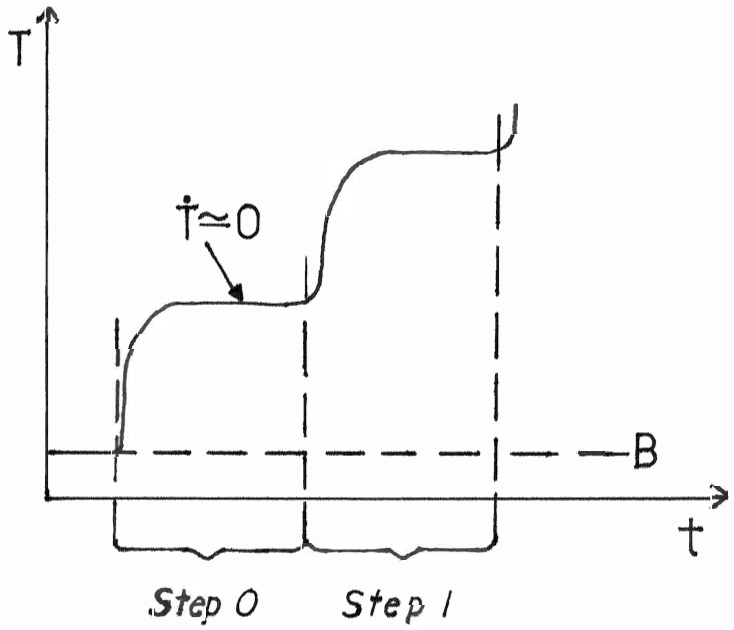

Figure II.2

can be obtained from the diffusion equation (II.1) when the time rate of change of sample temperature is zero. Using this information the heat capacity of the sample is calculated using the solution of the diffusion equation for C (equation II.3).

Recall now that we have been dealing with the simplified case depicted in figure II.1. However the actual apparatus is more complicated and is better represented by figure II.3. The sample as discussed so far is actually a sample, a strain gauge used as a heater and a thermometer element all adhered with some General Electric (GE) 7031 electrical varnish on a sheet of OFHC (oxygen free high conductivity) copper (see section I for details). Consequently the heat capacity measured is the total heat capacity of all these materials. The total heat capacity excluding the sample's, must be subtracted as addenda from the measured heat capacity. This can be done by either of two approaches, if the specific heats of the additional materials are well known then their heat capacities can be computed. However the simpler approach is to perform an additional measurement of the heat capacity without a sample mounted. This measurement should be performed with some regularity to ensure the integrity of the results.

As shown in figure II.3 the configuration is quite complicated, with each element at their own temperature and individual thermal conductances between any two materials which are in contact. In fact this diagram still falls short of telling the true story

Figure II.3, Detailed Thermal Schematic

B: copper bath, C: copper mount sheet,
H: strain gauge heater, K: any thermal link,
L: liquid bath, P: power supplied (Joule heat),
R: thermal radiation, S: sample, T: thermometer.

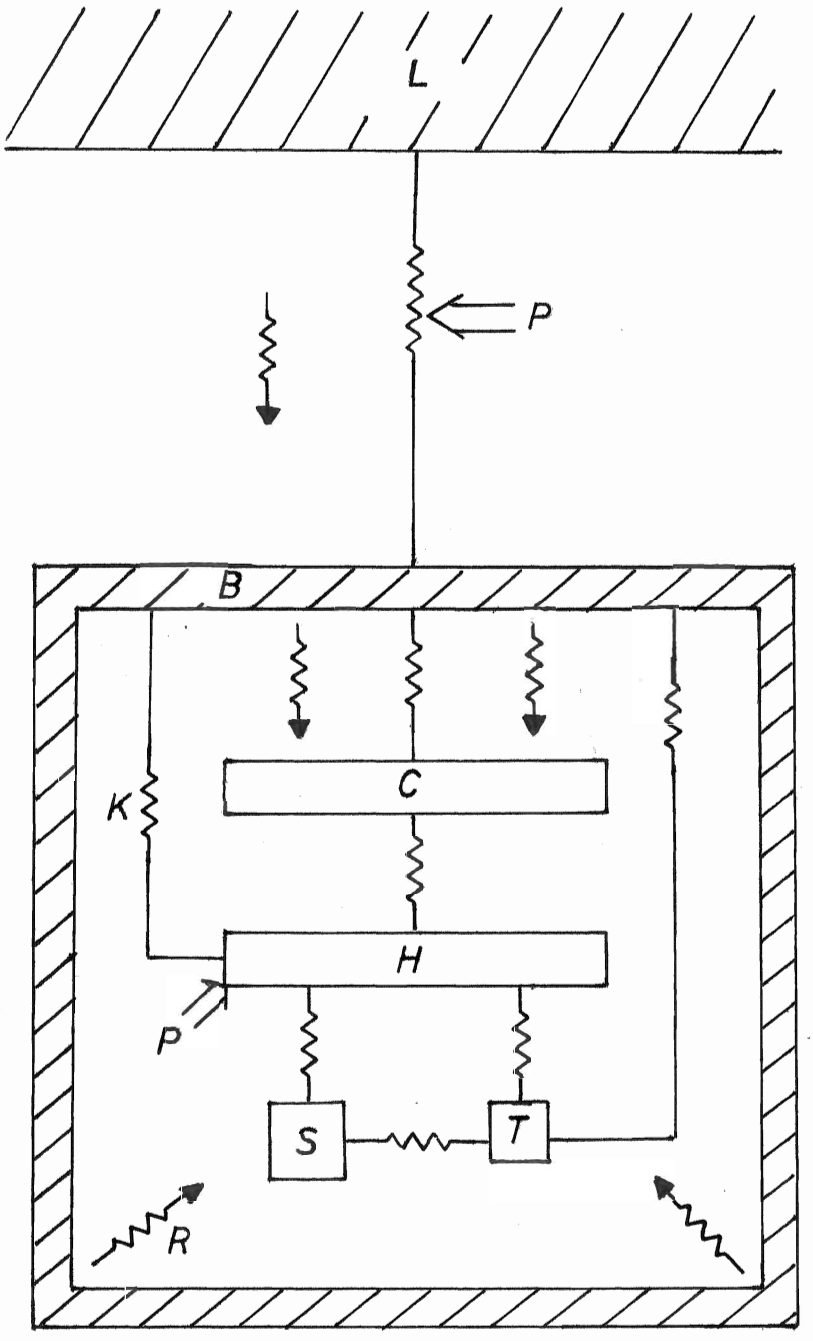

Figure II.3

since the varnish is not included. However the intention of the design is to obtain the best possible thermal contact between all the materials mounted on the OFHC copper sheet. Then the conductances between them are large (all the materials are good thermal conductors with the possible exception of the sample) and thus can be considered as a single body at one temperature. The heat capacity is then the total heat capacity due to all the contributions from these materials. This one body is well isolated from the bath by some weak thermal link comprised of the wires forming the electrical connections necessary to make measurements and provide Joule heat, and a long (~15 cm) heavier gauge wire (no. 30) serves as the primary thermal connection to the bath. Thus the effective thermal conductance in the diffusion equation (II.1) is that due to these connections and thermal radiation, if present. This was believed to be an advantage of this technique, since the conductance is estimated frequently (once for each measured value of heat capacity) it should readily account for thermal radiation.

The so called bath is a large copper mass, the temperature of which is controlled allowing measurements could be performed over a wide temperature range (~4.2K to 300K). The whole system is then placed in an appropriate liquid bath to cool the apparatus to low temperatures. This further complicates the apparatus since there is now another thermal conductance between the liquid bath and the bath (large copper mass), and another source of Joule heat. However this conductance is very large to ensure

that the system will reach sufficiently low temperatures (≈4.2 - 5K) and the heater then serves to isolate the bath from the liquid bath. The power supplied to this heater is provided by a temperature controller. The heat flows from the copper mass to the liquid bath since the copper mass will always be at a higher temperature than the liquid bath. Therefore the power supplied to the copper mass that doesn't heat the mass, is lost via the thermal link to the liquid bath. It is concluded therefore that we can disregard the liquid bath and this thermal conductance in the thermodynamic analysis of the system. Also, the link between the sample and bath is weak and therefore small rapid fluctuations in bath temperature should not affect the sample temperature significantly. That is, the fluctuations in bath temperature are attenuated like the voltage of an R-C circuit.

In summary, the measured heat capacity is the total heat capacity of all the materials mounted on the copper sheet, including the sheet itself. The effective thermal conductivity is that due to all conducting paths back to the large copper mass which is continuously maintained at a constant temperature by independent temperature controllers.

II.2. Method

The modifications to the method of Depuydt and Dahlberg [1] lie primarily in the addition of the secondary heating stage. The principle then is to use the temperature controller(s) to establish a fixed temperature of the copper mass. This heat

reservoir then is taken to to be the so called bath which is analogous to the liquid Helium bath in the analysis of DePuydt and Dalhberg [1].

The basic procedure is as follows;

1) Establish a set point and a tolerance window for the copper bath.
2) Ensure that the bath and sample temperatures are stable by checking that both temperatures fall within the temperature window for a fixed period of time (usually 3 minutes).
3) Once stable, supply the specified amount of power to the sample for the first heating step (ie. until $dT/dt \cong 0$).
4) Using this final temperature, estimate the effective thermal conductance of the link between the sample and bath (II.5).
5) Increment the power to the next desired level, that is ,

$$P_n = P_{n-1} + \Delta P, \qquad \text{(II.7)}$$

where ΔP is the desired power step.
6) Record the temporal response of the sample (temperature vs. time data) of the resulting heating step again until $dT/dt \cong 0$.
7) Estimate the effective thermal conductance at the end of the heating step using the conductance equation (II.5).
8) Using this and the previous value of thermal conductance, along with the linear interpolation formula for K[T(t)] (II.6), compute the total heat capacity for that heating step (from equation II.3).
9) Repeat steps 5 through 8 until the sample is at or above the

next desired bath temperature.

10) Set new bath temperature and repeat steps 2 through 9 until all bath set points have been processed.

This procedure is executed entirely by computer, following a sequence specified by the user. This program is outlined in appendix A [12a], although some important aspects will be discussed in this section.

Central to the heat step method is the acquisition of the temperature versus time data during the heat step. The first consideration is how to determine when a heating step is considered to be complete. More specifically, when is dT/dt sufficiently close to zero to maintain the desired experimental accuracy (~1%). DePuydt and Dalhberg [1] do not state explicitly how this is done, but it appears that they assume that some fixed period of time is sufficient for the temperature to stabilize and the system to reach a new thermodynamic equilibrium. This approach requires that the minimum time for stability be experimentally determined prior to the heat capacity measurements. Hence the experimenter must, in advance, have some idea as to the temperature at which the sample's heat capacity would be at a maximum. Then the time required at this temperature for the required conditions to be met must be measured. This is the problem of this approach, since the sample's heat capacity is not be known as a rule, the method has significant defects.

A better approach is to use a computer algorithm to detect when the condition, $dT/dt \cong 0$ has been satisfied. At this time the system is in its new thermodynamic equilibrium. A criterion must be established to govern the detection of dT/dt sufficiently close to zero to preserve the desired accuracy. This will be referred to as the stability condition. The approach taken then was to check when the ratio of change in temperature of the most recent two readings to the total change in temperature from the beginning of the heating step to the most recent reading is sufficiently small. That is, if the last temperature is T_i, and T_o is the initial temperature of the present heating step, the relative change is,

$$\Delta T_{rel} = (T_i - T_{i-1})/(T_i - T_o). \qquad (II.8)$$

It must therefore be determined what value of ΔT_{rel} is sufficiently small. This was accomplished with two programs [12b] which generate artificial temperature versus time data and then use this data to recompute the values of heat capacity and effective thermal conductance used to generate the data.

The value of ΔT_{rel} was adjusted until the computed heat capacity agreed with the chosen value to within 0.1%. 0.1% was used so that when this error was compounded with other sources of experimental error the overall error would be less than 1%. The magnitude of these other errors are difficult to estimate since some of the data is used in a numerical integration.

It was found however that the required value of ΔT_{rel} was beyond the limits of the experiment, that is ΔT_{rel} is small compared to the measuremental resolution. Also this method will proceed after the first event which satisfies the criteria. Consequently, depending on the time interval, the criteria may be prematurely met and introduce errors well in excess of the desired accuracy. This postulate is supported by the small value required for ΔT_{rel}.

Therefore rather than terminating the data generation the first occurrence in which the stability condition is satisfied, several sequential occurrences are required for termination. In fact this is improved on by computing the relative change over a range of values with the range increasing as the condition is repeatedly satisfied. In other words ΔT_{rel} is redefined as,

$$\Delta T_{rel} = (T_i - T_{i-k})/(T_i - T_o). \qquad (II.9)$$

Thus initially k = 1 and is incremented each time $\Delta T_{rel} < \Delta T'$ where $\Delta T'$ is some adjustable value chosen as detailed below. If however $\Delta T_{rel} > \Delta T'$, k is reset to 1 and the process repeated. Processing is terminated when k reaches k', that is k' sequentially occurring temperatures that satisfy the condition, $\Delta T_{rel} < \Delta T'$.

It is then necessary to determine the combination of k' and $\Delta T'$ which preserves the desired accuracy, while keeping ΔT_{rel} large enough to be obtained experimentally. Since the experimental limitations cannot be adjusted, the value of $\Delta T'$ must be

constrained to

$$\Delta T' \geq \Delta T_{min} / \Delta T_{step} , \qquad (II.10)$$

where ΔT_{min} is the instrumental resolution and ΔT_{step} is the magnitude of the heat step. The magnitude of the instrumental resolution increases with increasing temperature, but typically the rate of change of heat capacity decreases. Therefore as the temperature increases the size of the heat step can also be increased. The following table gives the typical values for these parameters for each functional temperature range as dictated by the Lakeshore DRC-91C temperature controller used in the final configuration.

Table II.1

Temperature	ΔT_{min}	ΔT_{step}	$\Delta T_{min}/ \Delta T_{step}$
1.500 - 9.999K	0.003K	0.30K	0.01
10.00 - 99.99K	0.015K	1.5K	0.01
100.0 - 450.0K	0.03K	3.0K	0.01

The data in this table are typical values used with experiments using the Lakeshore DRC-91C temperature controller with a precision calibrated Si diode temperature sensor. However these values are not necessarily applicable to all experiments performed.

The programs to generate artificial data and recompute the initial values were modified to reflect this new procedure and this time k was adjusted to obtain the desired accuracy. This computer experiment gives k' = 30 and $\Delta T'$ = 0.01 for a 1.4% accuracy in the recomputed values for heat capacity.

In order for these programs to provide a proper test, the data generated should represent a realistic temporal response. To do this, an appropriate function using realistic values of heat capacity, power and effective thermal conductance is needed. This function is obtained from the diffusion equation (II.1) by solving the first order non-linear differential equation for temperature as a function of time. If the heat capacity, C, and effective thermal conductance, K, are taken as constant for the period of time over which the equation is solved, the differential equation takes the form,

$$y' + f(x)y = g(x). \qquad \text{(II.11)}$$

Using the solution of II.11 with appropriate substitutions,

$$T(t) = T_B + P/K\ (1-e^{-Kt/C}) \qquad \text{(II.12)}$$

is the solution of the diffusion equation (II.1) for sample temperature. This solution of course has limited application but serves well here to test the computation routines that will eventually be used with experimental data.

Some additional aspects and flowcharts of the data generation program and the heat capacity program are provided in appendix B [12b].

II.3. Observations and Discussion

Since this method did not work, this section is approximately a chronological account of the efforts made to produce a functional and accurate system. With each modification or analysis

performed, a short discussion provides the reasoning for the attempt, observations and results. Where it was believed understood, an explanation for the failure of the attempt is provided.

The first experiments were performed using design 1 of section I. First cryostat performance was evaluated through a few qualitative experiments. When the cryostat was cooled to near liquid helium temperatures (7.4K), the inside temperature remained fairly constant for about 11 hours at which time the temperature was just above 10K. During the next 12 hours the temperature increased in two steps to approximately 240K. These observations indicate that the cryostat chamber walls provide sufficient thermal isolation for a long liquid helium lifetime. However, the minimum temperature attained was only 7.38K while the liquid bath is at 4.2K. This result indicated that the thermal coupling to the liquid bath was insufficient. However recall the inner chamber was in two sections a slightly wider stainless steel tube for the upper portion and a copper tube in the lower portion. The cup was designed to fit the smaller copper section which has only its upper ~2" in direct contact with the liquid bath. By ensuring that the coupling takes place in this region the bath temperature could be reduced to 6.2K. This was the lowest temperature reached with design one, the 2K difference likely due to thermal leaks to room temperature. If required, lower temperatures would have been possible by pumping on the liquid helium chamber.

Accepting these temperatures as limitations of this cryostat, the the selection of a sample temperature sensor was the next task. Various uncalibrated sensors were available in the lab. By use of the Scientific Instruments temperature controller with its calibrated sensor and the N-cal automated calibration program [12d] these sensors were precisely calibrated. After examining the response curves of an Alan-Bradley, carbon glass, Fe-Au thermocouple and a Ge diode, the Fe-Au thermocouple was selected since it provided the best response rate and linearity over the desired temperature range of 5-300K.

Trial runs were performed at liquid nitrogen temperatures (lower cost) to test control program performance, temporal response and heat capacity (~47 mg Cu used as a test sample). To obtain a smooth temporal response, the power step size was increased to correspond to a temperature interval of about 1.5K from about 0.3K. Without the increase, the instrumental resolution was about 2-5% of the step size, resulting in a visibly discrete heating curve (see figure II.7). This results in premature satisfaction of the stability condition due to a sufficiently large sequence of data that has been truncated to the same digital value. With a larger step, the resolution becomes relatively small and the stability condition satisfied at a more appropriate time (ie. dT/dt closer to 0). The result is the accumulation of a few hundred data points per step rather than 50-100 points. The increased step was also anticipated since the

heat capacity in this temperature range should be much larger than observed at the lower temperatures of DePuydt and Dahlberg [1].

The measured heat capacity as a function temperature was found to have large fluctuations (as great as 20%). These fluctuations were observed to decrease with increased step size. This dependence is also evidenced by the continuous increase in the magnitude of the fluctuations as individual experiments proceeded to higher temperatures (the heat step reduced due to the increased heat capacity). Also observations on separate experiments of different step sizes supported this conclusion. Examining the temporal response curves, (produced by screen dumps at the end of each heating step) it was seen that the initial temperature of one step was somewhat higher than the final temperature of the previous step. This difference in temperature was observed to be on the order of 10% of the temperature step. A correlation between the fluctuations and the temperature difference is not obvious, but the data analysis does assume a zero temperature difference between the end of one step and the start of the next. This apparent temperature drift could not be eliminated by modifying the stability condition since tightening the constraint made the stability condition experimentally inaccessible.

The approach adopted was to reduce the time interval between steps. The program was structured to obtain the largest possible

number of data points during a heat step at constant time intervals, therefore the voltages were not converted to temperatures until after the heating step was complete. The stability condition could be tested equally well using sensor voltage since the response curve was nearly linear over the full range and certainly piece wise linear in the temperature interval of one heating step. However the conversion routine was sufficiently efficient that each voltage could be converted to a temperature during the 1 second interval between temperature measurements. Now at the end of each heating step the data only was plotted and saved to disk. This reduced the temperature error at the beginning of each step but did not significantly affect the final heat capacity data. Finally compiled basic, which is faster than interpreted basic, (previous programs were interpreted) was used, which reduced the temperature jump to the order of the instrumental resolution. However, these improvements had a negligible effect on the fluctuations in the heat capacity.

It was also observed that the sample temperature was typically colder than the bath temperature when the bath was heated above the liquid bath temperature (table II.3). When the sample mount was removed from the cryostat, the wires were found secure and unable to make physical contact with the chamber wall. The reduced temperature therefore was due to thermal radiation, hence a radiation shield was introduced.

Table II.2
Effect of Thermal Radiation
on Sample Temperature

Bath Temperature (K)	Sample Temperature (K)	Difference (K)
78.8	78.2	0.6
100.0	89.7	10.3
150.0	110.3	39.7

The drift itself was then considered to be the source of the heat capacity fluctuations. That is, the analysis requires that at the end of each heating step the rate dT/dt must be zero so that the thermal conductance can be estimated. Some authors found that the introduction of a radiation shield reduces drift which may then allow for a more stringent stability condition to be satisfied experimentally.

For these two reasons, attempts were made to produce a radiation shield for this apparatus. The shield was designed to be of low mass and in excellent thermal contact with the bath so that the bath heater alone would be sufficient to control bath and shield temperatures. A thin OFHC copper sheet was rolled in a slightly conical shape, tapering towards the bottom end of the shield. The wires running from the bath to the sample mount were passed through groves on the side of the bottom section of the copper bath so that when the copper sheet was slide onto the bottom end of the bath, a large contact area was achieved (Apiezon grease was used for improved contact). The bottom of the shield was not

capped since the mount was at a large distance from the bottom of the cryostat compared to the chamber wall and the sample was hung vertically, so that the effective cross section was small.

This shield design did not work well because the chamber was too small. It was impossible to prevent either the wires from thermally shorting to the shield, thereby increasing the thermal conductance back to the bath from the sample, and/or the shield from shorting to the chamber wall, thereby making the shield ineffective. It was therefore decided that a new calorimeter should be constructed.

The new calorimeter is essentially design 2 of section I. The early version differed slightly from that described in section I in that both support posts were intact and brass screws were not placed in the brass flange to provide additional and more effective wire thermalization. Also since both support posts were intact a heater coil was wrapped around the bottom of both posts. The two coils were made from one wire wound down one post and up the other. The section of wire bridging the space between the posts was a bent no. 30 copper wire so that no tension is created as the wires heat and to maximize power transfer to the posts.

The shield of this design is a considerably more massive copper cylinder, with a larger surface area exposed to thermal radiation then the one used in design 1. Therefore, a separate heater must

be used to control the shield temperature to match the bath temperature. The simplest approach is to use a voltage divider style circuit to balance the proportion of power supplied to the bath and shield heaters provided by one controller. However the controller's power output is insufficient to drive the large load with optimal power transfer. Therefore a power amplifier is required to boost the power. Secondly, this scheme works well only in a narrow temperature range requiring that the variable resister use to adjust the balance must be re-adjusted for different ranges. The latter problem defeats our goal of producing a fully automated calorimeter useful over the temperature range of 5-300K.

It is however difficult to determine how the system will respond because the shield is not in direct contact with the liquid bath except through thermal radiation. Rather the shield is in physical contact with the heated bath which in turn is in direct contact with the liquid bath. The thermal conductance between the bath and shield is not predictable since it is a function of both the bath and shield temperatures which are both changing. However it is possible that a proportional amount of power to the shield may work. This aim can also be achieved by driving the shield heater with a power amplifier the output of which is proportional to that supplied to the bath heater (ie. $P_2 = \alpha P_1$).

Surprisingly, it turns out that the gain can be adjusted such that this method works very well. The lag in temperature of the

shield seemed to affect the bath temperature in such a way as to reduce the time required to stabilize the two temperatures. However, as suspected, the magnitude of this gain is a function of temperature, making the method difficult to automate.

An analog circuit (figure II.4(a)) was designed to adjust the power supplied to the shield heater in response to the power supplied to the bath heater and the temperature difference between the bath and shield. The circuit's theoretical output was given by,

$$V_2 = \alpha \{|½V_1 + \beta V(\Delta T)| - V_D\}, \qquad \text{(II.13)}$$

where V_2, V_1 are the voltages supplied to the shield and bath heaters respectively, $V(\Delta T)$ is the differential voltage proportional to the temperature difference and V_D is the diode voltage. α and β are adjustable proportionality constants designed to gauge the circuit response to the thermal characteristics of the apparatus.

The development of a properly functioning circuit proved a formidable task, the temperature difference was sensed using the obvious choice of a differential thermocouple (Cu-constantan). Although the circuit worked outside the calorimeter, once inside, the thermocouple appeared to pick up high frequency noise and this was somehow rectified in the circuit. This combined with the high gain required for the small thermocouple voltage, railed the op-amps in the circuit rendering the circuit useless. Many attempts were made to reduce the noise with filtering and

shielding or offsetting the amplifier, but the circuit would not work as desired. The thermocouple was then replaced with a resistance bridge using two thin film platinum thermometers and two precision resisters on the circuit board (figure II.4(b)). With this arrangement the voltage applied across the bridge could be set large enough that a much lower gain could be used. The contribution due to noise becomes negligible. The accompanying Joule heat does not significantly affect the shield and bath temperatures due to their large masses and strong thermal links to the liquid bath.

As it turned out, the circuit design cannot perform the desired task. At room temperature the circuit worked very well with the shield and bath stabilizing rapidly to the same temperature. In fact, the circuit seemed to shorten the time required to stabilize the bath at the set point, compared with the time achieved by the controller alone and no power supplied to the shield. However at liquid nitrogen temperatures the circuit required re-adjustment, exactly what we hoped to avoid. More critically, the circuit could not be adjusted such that the bath and shield stabilized at the same temperature. Once both were stable, a temperature difference existed. Upon analysis of the theoretical voltage across the centre taps of the sensor bridge, it is seen that if a small adjustment is needed to balance the bridge at one temperature then even if both sensors have the same temperature coefficient, a different adjustment is required at some new temperature. However this was known in advance and

Figure II.4, Master-Slave Heater Control Circuit

(a) Schematic of heater control. INA 102 is an instrumentation amplifier. The HP 6824 is a power amplifier with a 75W maximum power output. All other amps are IC's similar to the 741.
(b) Illustration of resistor bridge, the T's are thin film platinum thermometers and the R's are well matched precision resistors.

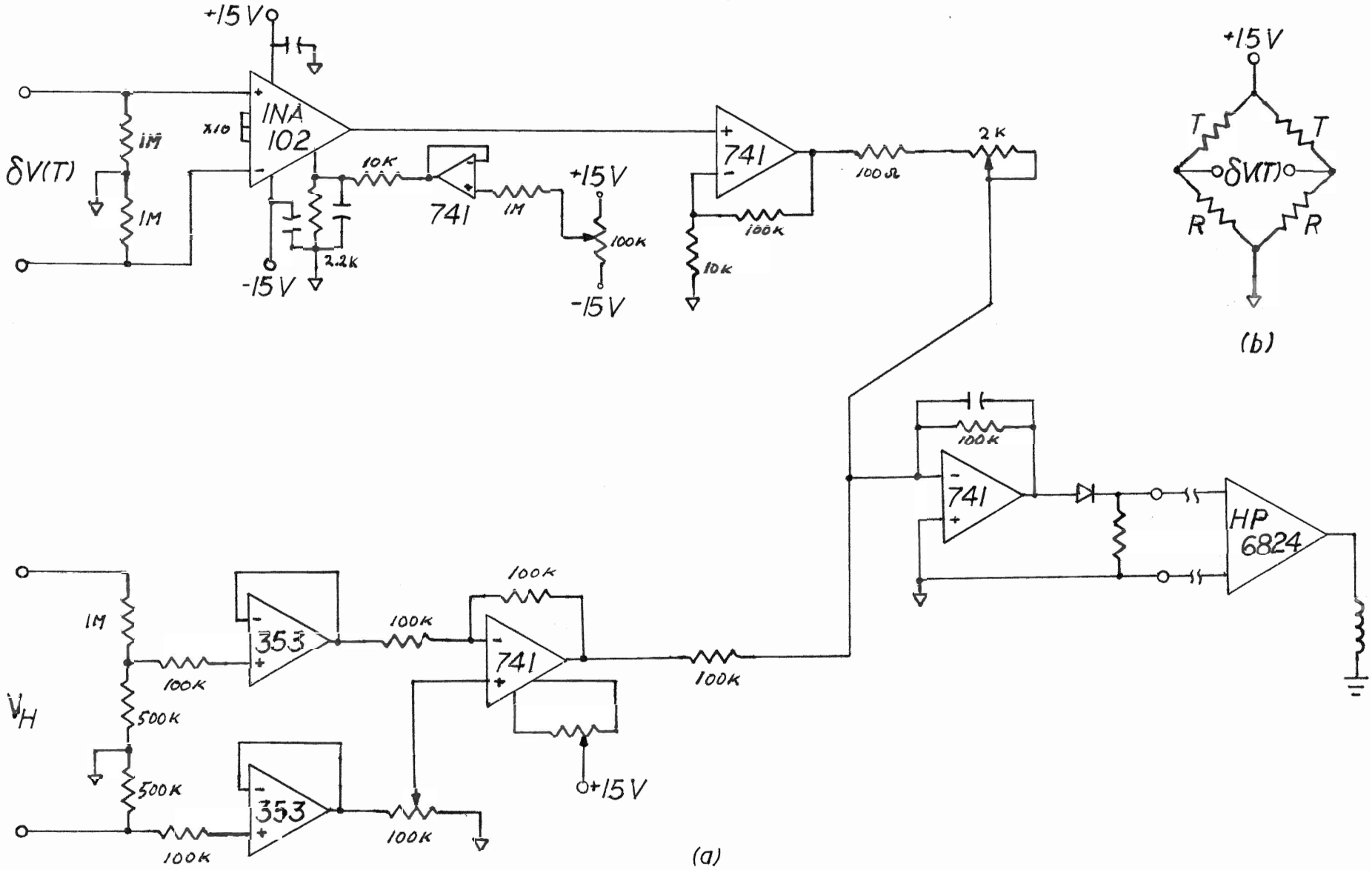
+15 V
δV(T)
1M
1M
x10
INA
102
-15 V
2.2k
10K
741
1M
+15 V
100K
-15 V
741
100K
10K
100Ω
2K
+15 V
T
T
δV(T)
R
R
(b)
100K
741
HP
6824
100K
353
100K
100K
741
100K
1M
100K
V_H
500K
500K
353
100K
100K
+15 V
(a)

Figure II.4

the elements were all closely matched to reduce this effect.

Consider however the circuit's response to the temporal evolution of the system. As the shield temperature approaches the bath temperature, the contribution due to this temperature difference reduces to zero leaving only the term proportional to the voltage supplied to the bath heater. As seen earlier this alone is not sufficient to match the two temperatures and thus the shield temperature begins to drift towards the temperature corresponding to that power output. Now the term for the temperature difference again becomes non-zero and drives the shield back towards the bath temperature. The temperature controller and this circuit engage in a battle which ends when some sort of thermodynamic and electrical equilibrium is reached somewhere in the middle of these temperatures. This is likely some temperature at which the contribution from the temperature difference is sufficiently small to be ineffective as a control parameter. This implies that increasing the gain for this term should reduce the difference but in fact a large gain causes the shield temperature to oscillate about the bath temperature.

At one point during this study it seemed fruitful to take the time to perform a series of experiments to try to determine the empirical relationship between the powers required to stabilize the two temperatures at the same value. In these experiments the power of one heater was fixed while the power supplied to the second adjusted until a thermocouple across two masses indicated

a temperature difference less then 0.1K. The temperature reached and the two powers were then recorded. The results of this analysis are displayed in figure II.5. A numerical analysis using least squares of different functions of both heater powers gives,

$$P_2 = 0.166 \exp(0.106\ P_1)$$

$$\text{or} \qquad V_2 = 3.48 \exp(1.5\ V_1^2), \qquad \text{(II.14)}$$

for the best fit to the data (V's are corresponding voltages). A fourth degree polynomial will also provide a reasonable fit to the data (figure II.6 and coefficients listed in table II.4).

Table II.3
Coefficients of Fourth Degree Fit

Term	0	1	2	3	4
Coeff.	0.188499	-0.00854	0.005928	-0.00027	0.000007

A circuit designed to follow this type of response would be somewhat involved and it construction time consuming. The experiments performed were also only performed in the same temperature range, therefore the temperature dependence, if any, of the coefficients is not known.

In conclusion it appears that the only way to effectively control temperatures, particularly when trying to have one temperature closely follow another, is to use a PID type controller. At this time however much time had been spent on the above circuit so it was decided that manual adjustment was the best approach at least until the heat capacity measurements themselves were working

Figure II.5, Associated Power

Graph of power supplied to shield heater as a function of power supplied to bath heater. Fitted exponential curve.

Figure II.6, Associated Power 2

Graph of power supplied to shield heater as a function of power supplied to the bath heater. Fitted fourth degree polynomial.

Figure II.5

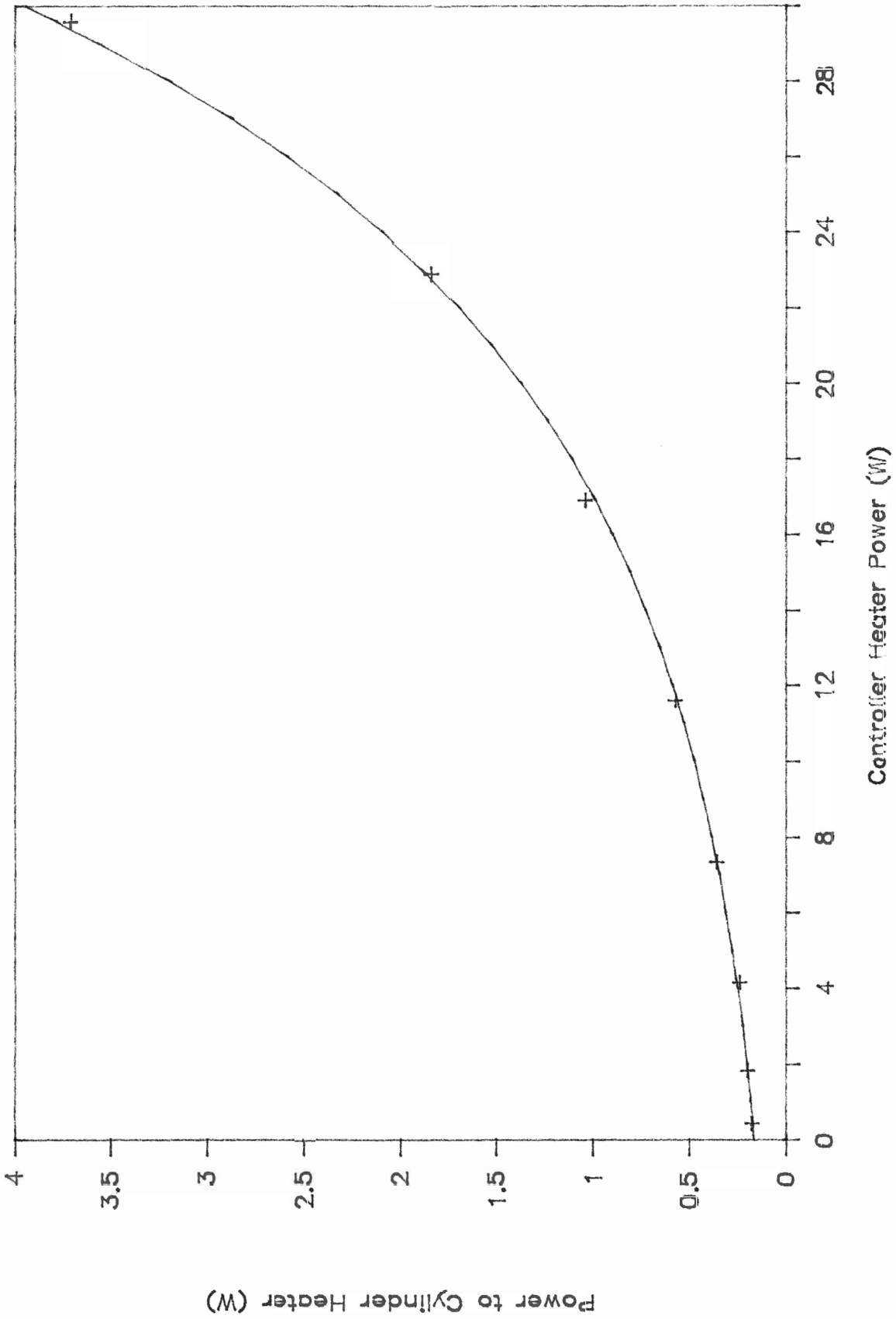
Power to Cylinder Heater (W)
0
0.5
1
1.5
2
2.5
3
3.5
4
0
4
8
12
16
20
24
28
Controller Heater Power (W)

Figure II.6

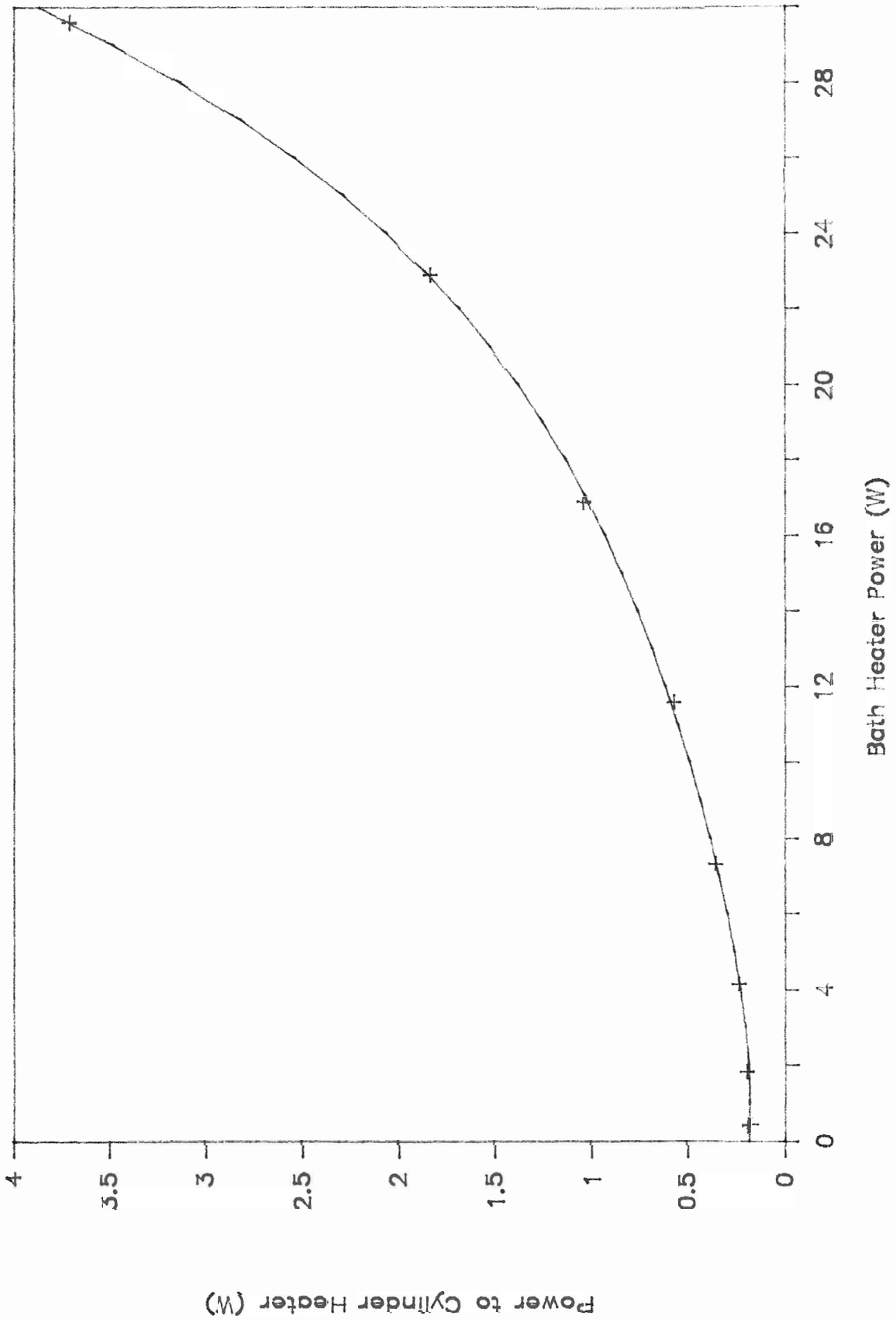
Power to Cylinder Heater (W)
4
3.5
3
2.5
2
1.5
1
0.5
0
0
4
8
12
16
20
24
28
Bath Heater Power (W)

well.

The focus is now again directed towards the heat capacity measurements themselves rather than to the peripheral functions required to automate the calorimeter over the full temperature range. With the new apparatus it was found that the Fe-Au thermocouple was too short to use properly. Specifically the length of wire remaining after travelling down the shaft to the sample chamber, was insufficient to achieve a small thermal conductance between the sample and bath, particularly since these wires are relatively thick and are excellent conductors. The iron-gold wire is also so soft that it often breaks as a result of the frequent assembly and disassembly required. The new thermometer must be kept small so that the addenda to the heat capacity is small compared to the sample's heat capacity. The response function must be sufficiently rapid so that a resolution of a few millikelvin is possible especially at low temperatures where the temperature step should be small since the heat capacity is generally small and varies more rapidly. The resolution must also be attainable with a small excitation current so that the Joule heat provided is small. A new temperature controller from Lakeshore Cryogenics was purchased along with a pair of Si diode sensors. It was also hoped that the use of a second controller would solve the problem of controlling the shield temperature. The DRC controller was equipped with a precision option which provides a resolution down to 1mK for T < 10K, with an accuracy of better than 10mK. The

controller is also capable of measuring up to 6 individual sensors (2 simultaneously) using a variety of sensor types. However to use the new controller, the program had to be modified to communicate with the DRC and reworked to reflect the data type (ie temperature in place of sensor voltage). Since modifications were necessary, the program was also modified to conform to those features unique to Quick Basic over GW Basic, which would improve on the programs efficiency and simplify any further programming.

With the new calorimeter vacuums on the order of 10^{-5} Torr could be achieved and, on cooling, the bath temperature would reach liquid helium temperatures soon after the liquid begins to persist on transfer (ie. rate of evaporation < rate of transfer). The shield temperature lagged somewhat behind the bath, reaching liquid helium temperatures 20-30 min after the bath, while the sample temperature lagged even further behind reaching its lowest value about a hour later.

The first design could easily reach room temperature when in a liquid Nitrogen bath and when in a liquid Helium bath, but this was at the limits of the heater. This new calorimeter however could not reach room temperatures when in a liquid Nitrogen bath. The thermal link to the liquid bath from the copper bath was too strong. This situation was remedied by cutting a section (~15mm) out of the support shaft which supported the electrical connector. A new heater was wrapped around the other shaft in the usual doubly-wound fashion. The required resistance was

still the same, so now the heater covered a length twice that of the original heater on that shaft. This provides a greater length over which the temperature gradient can occur. This combined with the reduction in the thermal conductance, allowed the system to be easily heated to room temperature when in liquid nitrogen. It was also observed that the sample temperature only cooled to about 17K with the original configuration. The wires coming from the top of the calorimeter were to be thermalized to the liquid bath's temperature by wrapping them several times around the top of both shafts. However some of the heat provided to the system heated this part of the shaft by about 7K despite its close proximity to the liquid bath. By installing two brass screws into the brass flange and re-wrapping the wires around these and the shaft that was cut, the bath could now be cooled to 9.9K. To further reduce the temperature difference, smaller wires were used below the connection point and the bath thermometer better installed. Specifically the diode sensor was mounted in a hole in the shaft (diameter just larger than sensor casing) and the lead wires wrapped three times around the shaft before proceeding to the connector. For these diodes, the element is in better thermal contact with the lead wires than with the casing). The sample could now cool to 4.9K.

A series of experiments, in which individual control parameters were tested, showed that using the digital filter of the DRC controller resulted in an increase of the observed fluctuations. The filter gives the average of the last 10 readings taken by the

instrument, this tends to reduce the effect of the digitalization by smearing out the discrete levels. The problem is the stability condition is not satisfied this way and the constraint had to be loosened so the experiment would take place program designed to wait for this condition).

As seen earlier, these new experiments showed again that the fluctuations in the heat capacity increased in magnitude with decreased power step size. Here steps of 0.5-1.0 mW showed marked fluctuations in C_p compared with that seen with steps of 1.5-2.0 mW. Also smooth well-resolved heating curves (fig. II.7) required 3mW power steps at 80K (corresponds to a temperature step of ~2.7K). Fluctuations in the conductance data, K(T), were observed while other data elements appear well behaved. The bath temperature was stable to within the digital resolution, individual heating steps showed an apparent smooth temporal response along with a smooth transition into the next heating step.

Another experiment was performed using a 3mW step with no digital filter, but the fluctuations in heat capacity data persisted. In this experiment the calculation of K(T) was modified such that a constant value was used for each step rather than using the linear interpolation. To better examine the effect of K(T) on the heat capacity, the raw data from the experiment (only data from steps between last 2 bath set points was available) was used to calculate heat capacity using a constant value for K

Figure II.7, Typical Heating Curve

Plot of a typical temporal response for a single heating step. A a 3mW step was used which results in ~2.3K temperature step at ~82K.

Figure II.7

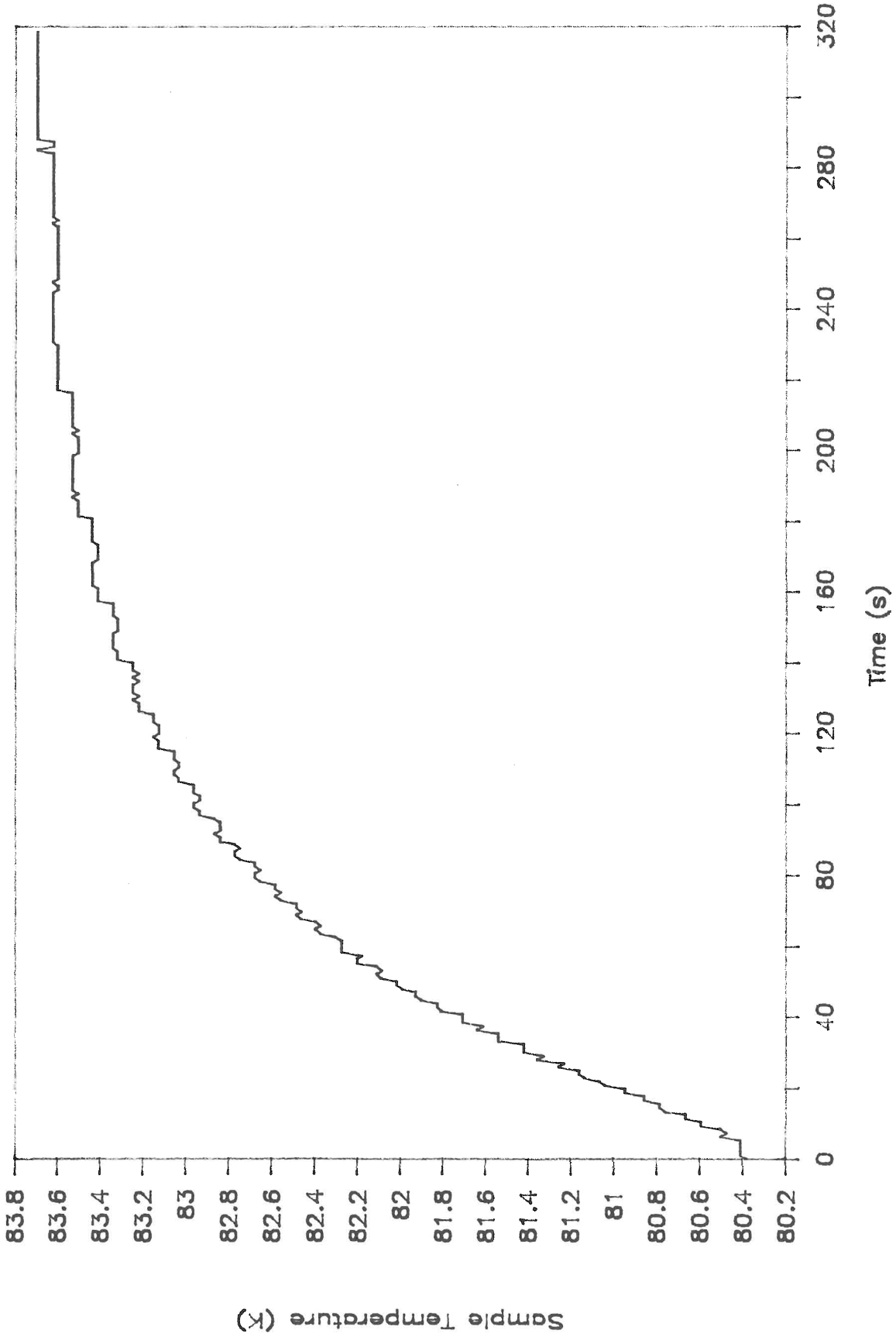
Sample Temperature (K)
83.8
83.6
83.4
83.2
83
82.8
82.6
82.4
82.2
82
81.8
81.6
81.4
81.2
81
80.8
80.6
80.4
80.2
0
40
80
120
160
200
240
280
320
Time (s)

throughout (the average of the values measured), K constant for each step individually (as above) and using the usual linear interpolation. The data was then compared to accepted values of heat capacity of Cu normalized to some median experimental value. The usual linear interpolation calculation, provided the best results. Fluctuations about the normalized accepted data, on the order of 1%, were observed for this experiment. The shape of the curve from this calculation most closely matched the expected response, as indicated by the accepted data. The data using individual constant values of K within each step showed much larger fluctuations of about 20%. Using a constant value throughout had smaller fluctuations but not surprisingly the data continuously diverged from the accepted curve.

Although this data shows some promise, the results using the usual calculation were unusually good and the number of data points here within one sequence (4 points) is clearly too small to draw any worthwhile conclusions. Therefore the program was modified to record, at the user's discretion, a full data set of the entire experiment. This file is usually large (for an experiment spanning 150K typically 1 Mb) but clearly required to properly evaluate the system.

Another experiment was performed, this time recording the full data set (fig. II.8). With the use of another program, SYS-ASC.BAS, this data was fully analyzed. Various data were plotted as functions of other parameters all demonstrating reasonable

behavior with the exception of the K(T). Examining the data it was evident that whenever a new bath temperature was established, a large error was seen in K(T) (fig. II.9). As the sample was heated however, the magnitude of this error decreased similar to an inverse function. This seems reasonable since $K = P/(T-T_B)$ and thus when the sample temperature is close to the bath temperature K becomes large, then as the sample temperature increases K decreases. This should of course be countered by the change in power as the temperature increases. However the error in K also goes as the inverse of the temperature difference, but when the errors are treated analytically, the maximum error is 0.9% while the largest error seen in K(T) is about 33%. This error is judged by assuming that the true conductance passes through the nearly straight line that K(T) seems to converge upon after each new set point. If the effect were simply an error, the data should fluctuate about this line. Instead after a set point is established, the error remains on the same side of the true curve until possibly the next set point. Some programing errors were discovered at this time but none had any serious effect on K(T) or C(T) results. The problems were corrected and results cross verified to be certain of their elimination.

The calculation of heat capacity was repeated using K(T) values computed from a line representing the estimated true curve. However the fluctuations were increased dramatically with the largest fluctuation at 300% and negative values occurring (fig. II.10). The implication here is that the K(T) curve observed is

Figure II.8, Heat Capacity vs Temperature

Typical heat capacity as a function of
of average temperature data. The vertical line divides
3mW and 2.5mW step regions.

Figure II.9, Thermal Conductance

Graph illustrates the large errors observed in the
thermal conductance as a function of final temperature.
The vertical divides the regions in which a 3mW and a 2.5mW
power step was used. The circled points are the first data
after a new bath temperature was established. The dashed
depicts the expected conductance suggested by the data.

Figure II.8

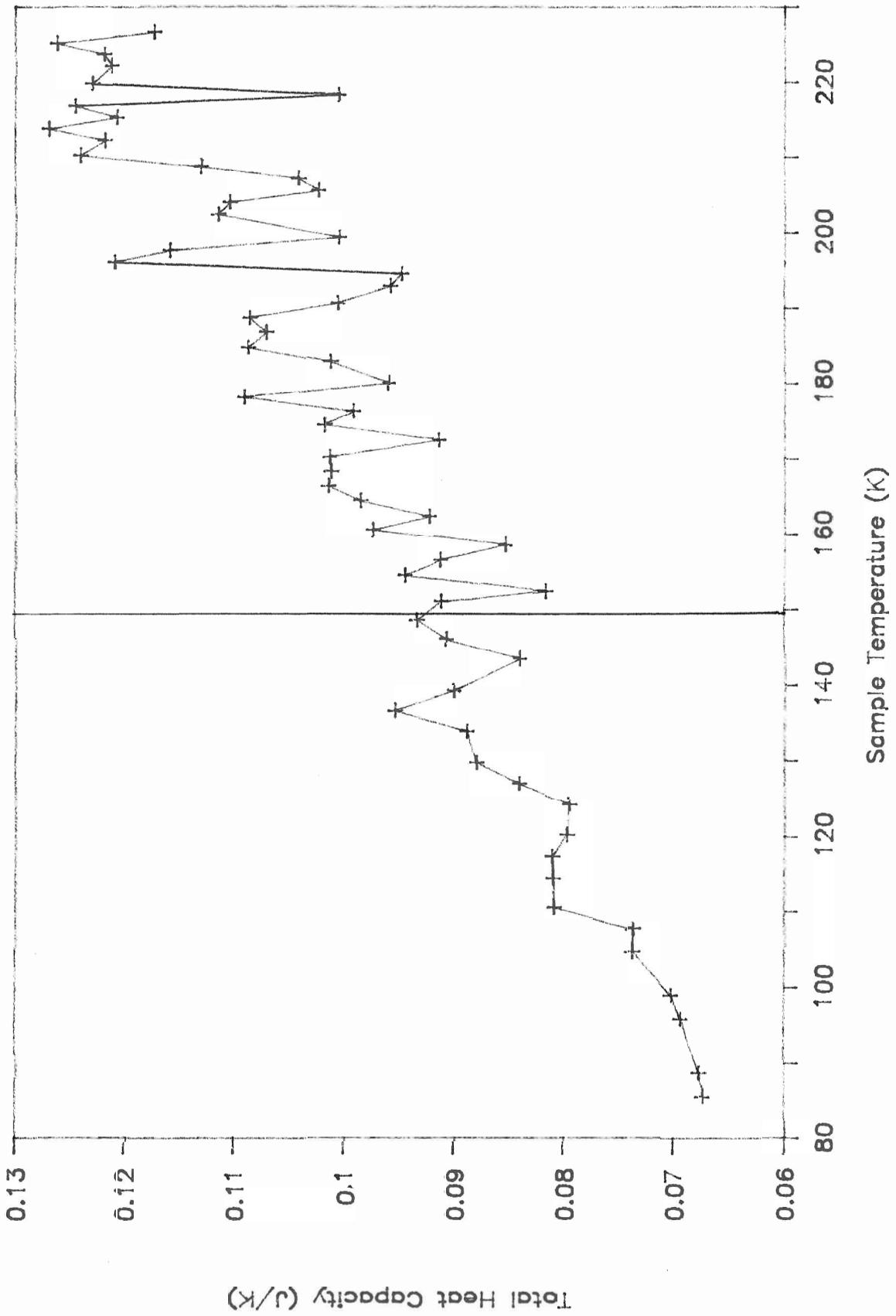
Total Heat Capacity (J/K)
0.13
0.12
0.11
0.1
0.09
0.08
0.07
0.06
80
100
120
140
160
180
200
220
Sample Temperature (K)

Figure II.9

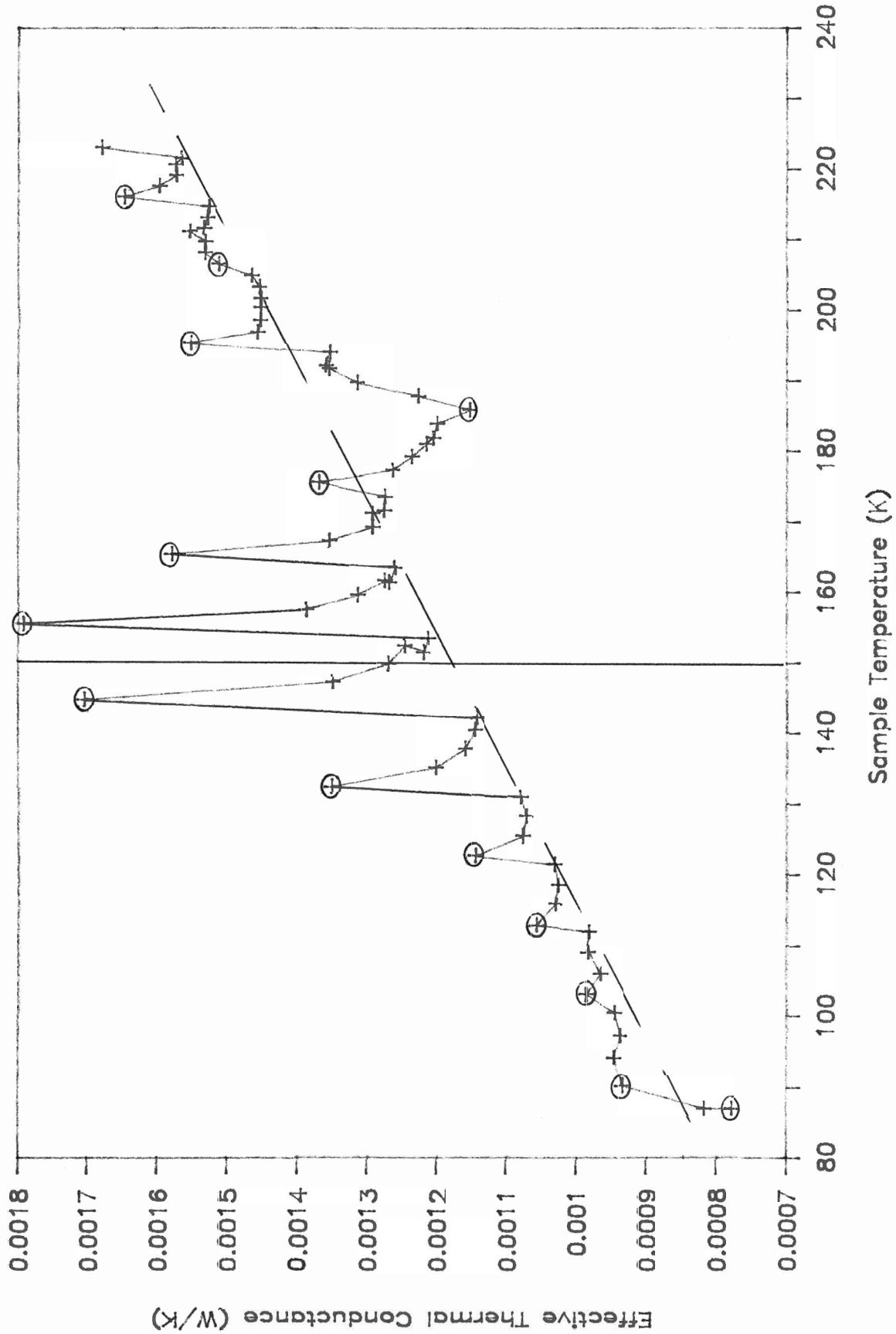
Effective Thermal Conductance (W/K)
0.0018
0.0017
0.0016
0.0015
0.0014
0.0013
0.0012
0.0011
0.001
0.0009
0.0008
0.0007
Sample Temperature (K)
80
100
120
140
160
180
200
220
240

actually correct despite its very unusual behavior. Additional support to this conclusion is provided when examining the heat capacity curves obtained by the usual calculation. No correlation between the C(T) fluctuations and the anomalies in K(T) is apparent.

There must therefore be some other factor affecting the estimate of K(T). That is we have assumed that the only important contact is via the various metallic paths to the bath. Thermal radiation is unlikely, its effects should increase as the temperature difference increases. A convincing explanation for the anomalies in K(T) was never determined, the fact that sometimes the anomaly shifts below the curve immediately eliminates the explanations considered. Accepting that the linear interpolation seems to provide the best results, other sources for the fluctuations in the heat capacity data must be considered. A more detailed investigation of the numerical analysis was performed next. We return to the data generation program to generate data which simulates noise, digitalization and both. Although the experimental data didn't implicate noise, the computer experiment is easy and worth while. The noise is simulated in the obvious way, namely a random number bounded by $-a < r < a$, is added to the values generated normally. The digitalization is simulated by truncating the normally generated values at some prescribed interval (15mK). The combination is performed by first adding the noise and then truncating. Both effects demonstrated fluctuations but neither was on the order of the the fluctuations

Figure II.10, Recalculated Heat Capacity

Recomputed heat capacities using various methods of computing the thermal conductance. Curve A was computed from the so called best fit line for the conductance data. Curve B was computed as usual and C computed with K constant for each step using the final value for each step.

Figure II.10

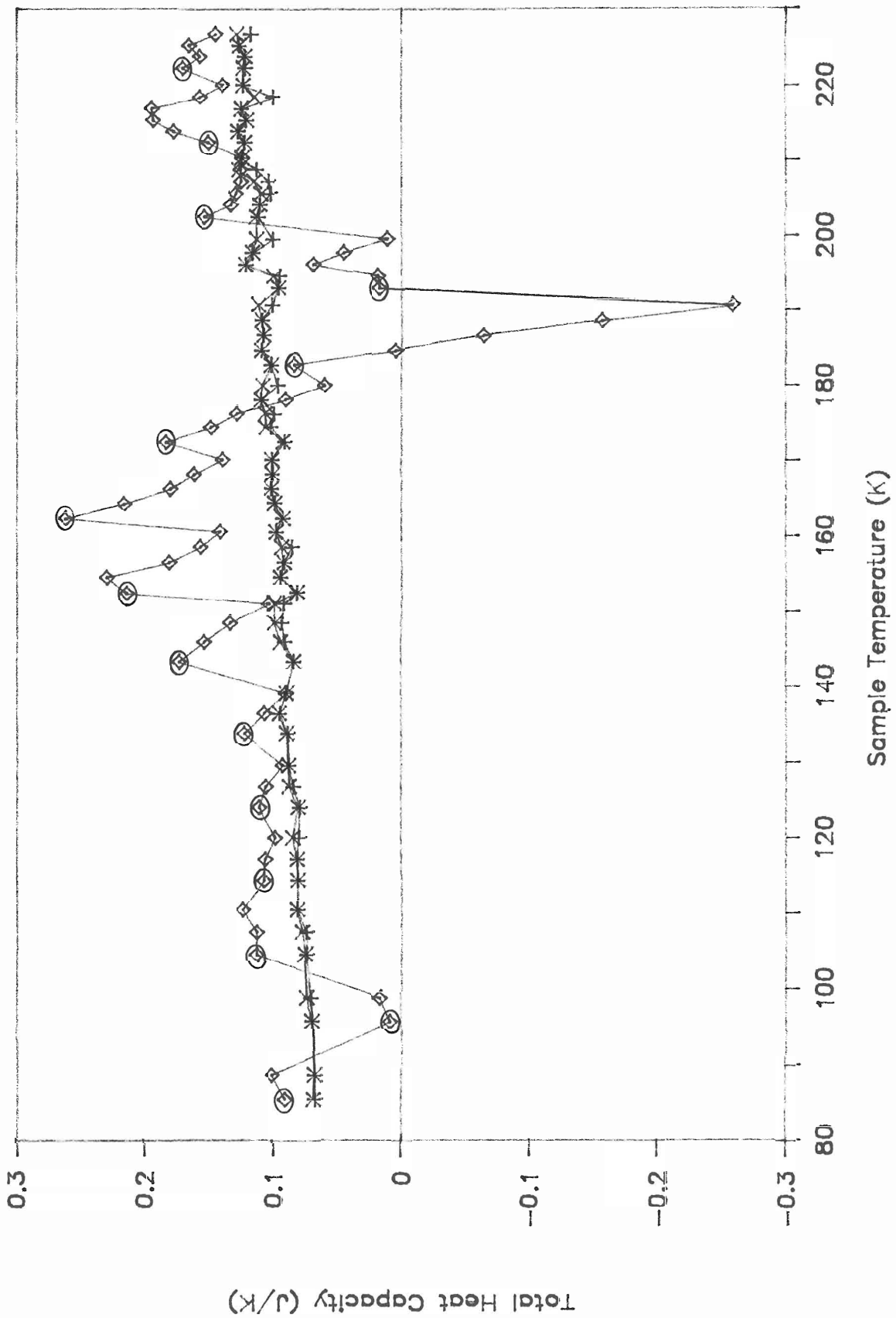
Total Heat Capacity (J/K)
0.3
0.2
0.1
0
−0.1
−0.2
−0.3
80
100
120
140
160
180
200
220
Sample Temperature (K)

observed experimentally (figure II.11). Also the experimental data typically showed fluctuations throughout, but the fluctuations found with the artificial data were intermittent or at least they were generally negligible. We conclude therefore that although contributing factors, the noise and digitalization alone cannot be responsible for the observed fluctuations.

These computer experiments did however point out a previously unnoticed problem. The temporal response curves produced artificially did not match the experimental data despite modeling the resolution and temperature after the experimental conditions (noise = ± 0.010K and resolution = 0.020K). The experimental data clustered in groups of 4 and then jumped an amount 4 times the resolution and repeated. This behavior was found consistent with a defective second bit of the analog to digital converter. When simulated, larger fluctuations were produced but they were very ordered, that is they consistently oscillated between -2% and -4% (fig. II.12). This can be understood by realizing that in the simulation the temperature step is constant, thus any effects related to the final temperature of each step could be repeated. Specifically here the data can be off by 1 times the digital resolution or 4 times the resolution, thus some temperature step could result in the final temperature switching between these values. The fact that the result is always less than expected is consistent with earlier observations on the effect of the numerical integration using unaffected data. However further experimentation after repairing the fault has had little effect.

All these corrections together have improved the performance but still not consistently to the desired level of <1%.

It was also speculated that some unusual effects may be occurring from the numerical integration method due to digitalization. The previous computer experiments indicate that this is not so, but to be certain the simpler trapezoid rule was used in place of the combined Simpson's 3/8 and 1/3 rules used so far (fig. II.13). The occasional data point was affected but fluctuations persisted and their magnitudes remained essentially unchanged.

The final consideration was that these effects would not be as significant at low temperatures (<20K). Experiments were performed at these temperatures with different power step sizes but the usual fluctuations still occurred.

Figures II.11 - II.13

Figure II.11, Effect of Digitalization

The upper curve is the unaffected computed artificial heat capacity. The lower curve is computed after imposing digitalization.

Figure II.12, Effect of Bit 2 Fault

The upper curve computed from unaffected data. The lower curve illustrates effect of bit fault.

Figure II.13, Simpson's vs Trapezoid

Plot of artificial heat capacities computed by Simpson's and Trapezoid rules for integration. The upper curve was shifted up buy a constant to separate the curves.

Figure II.11

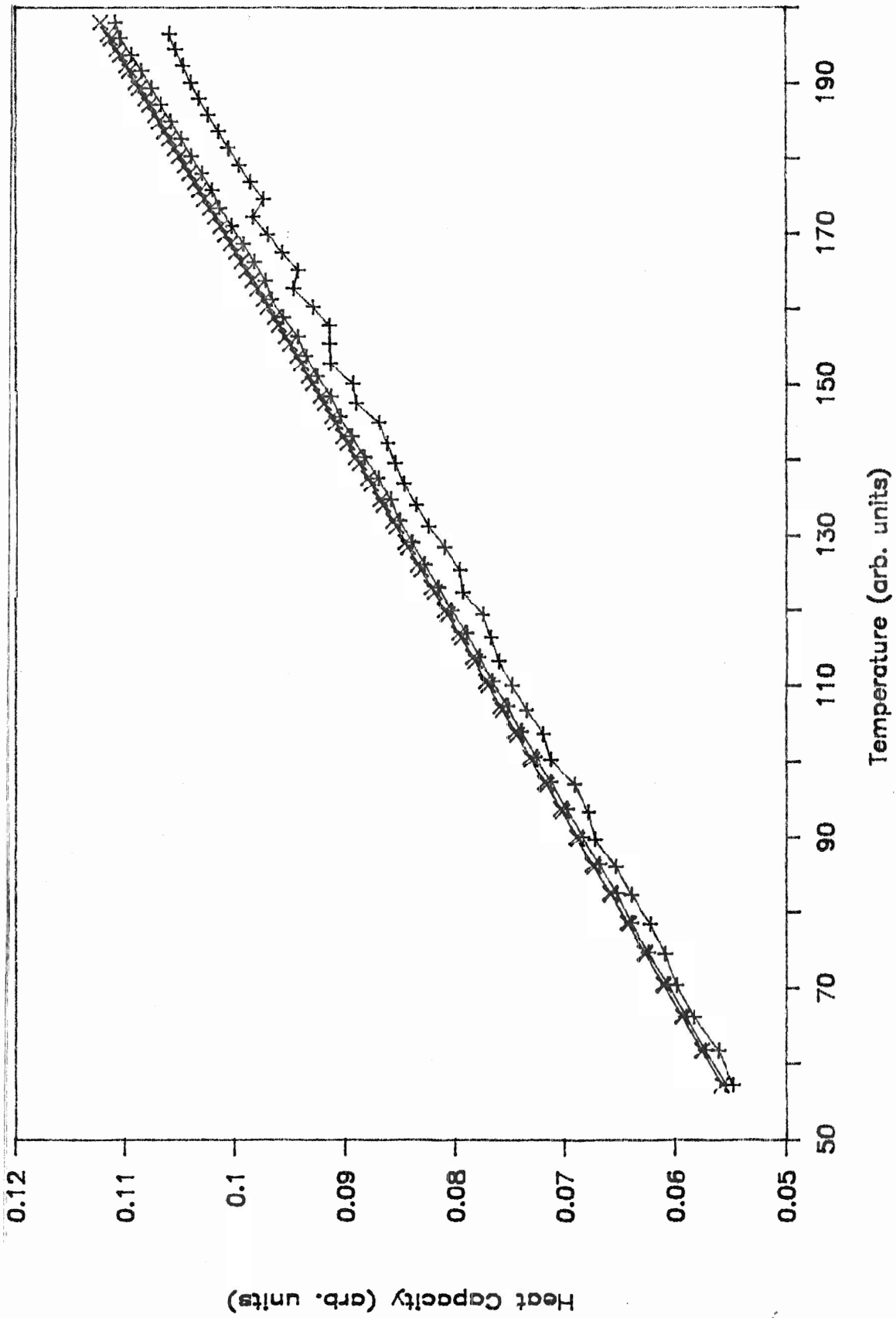
Heat Capacity (arb. units)
0.12
0.11
0.1
0.09
0.08
0.07
0.06
0.05
Temperature (arb. units)
50
70
90
110
130
150
170
190

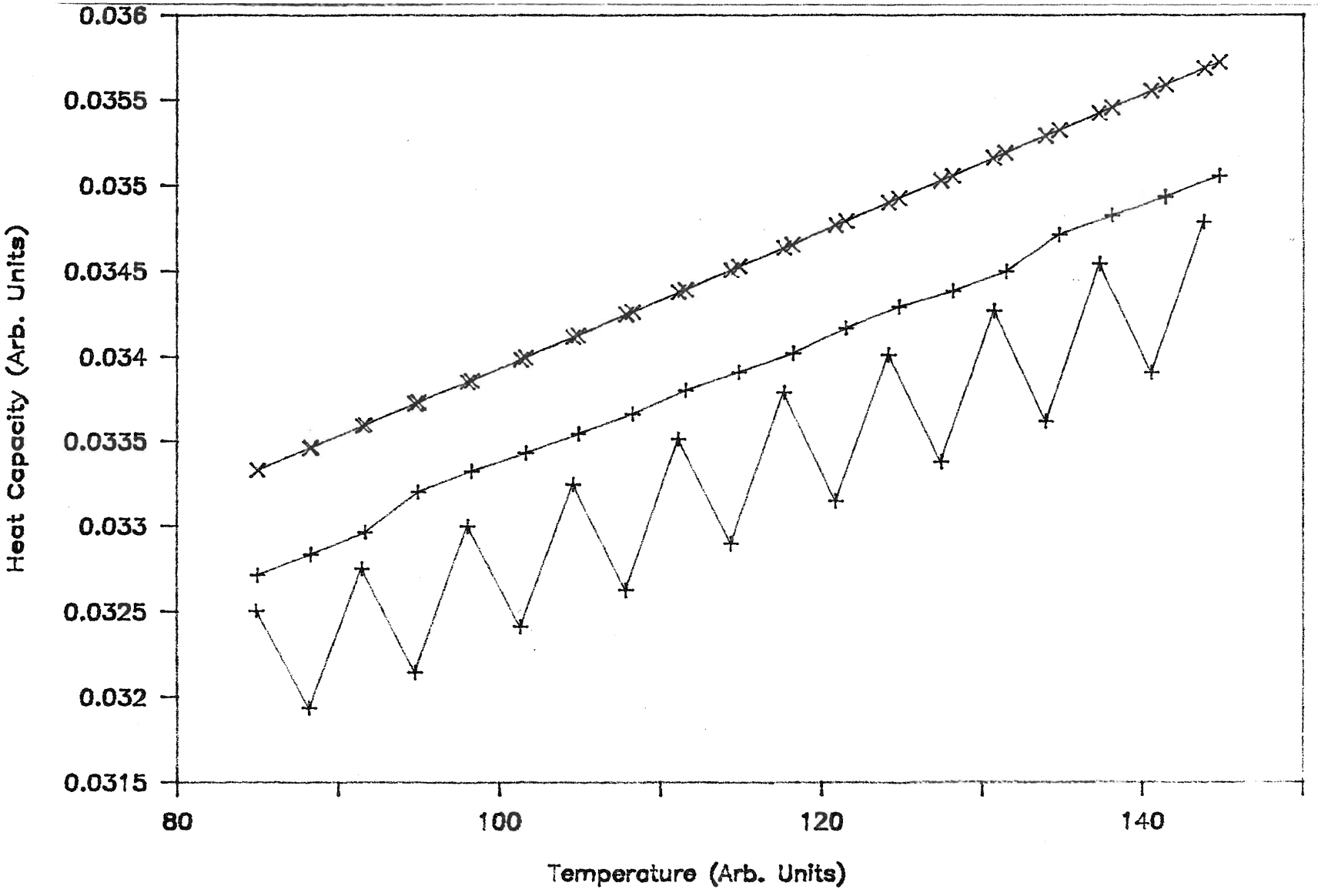
0.036
0.0355
0.035
0.0345
0.034
0.0335
0.033
0.0325
0.032
0.0315
Heat Capacity (Arb. Units)
80
100
120
140
Temperature (Arb. Units)

Figure II.12

Figure II.13

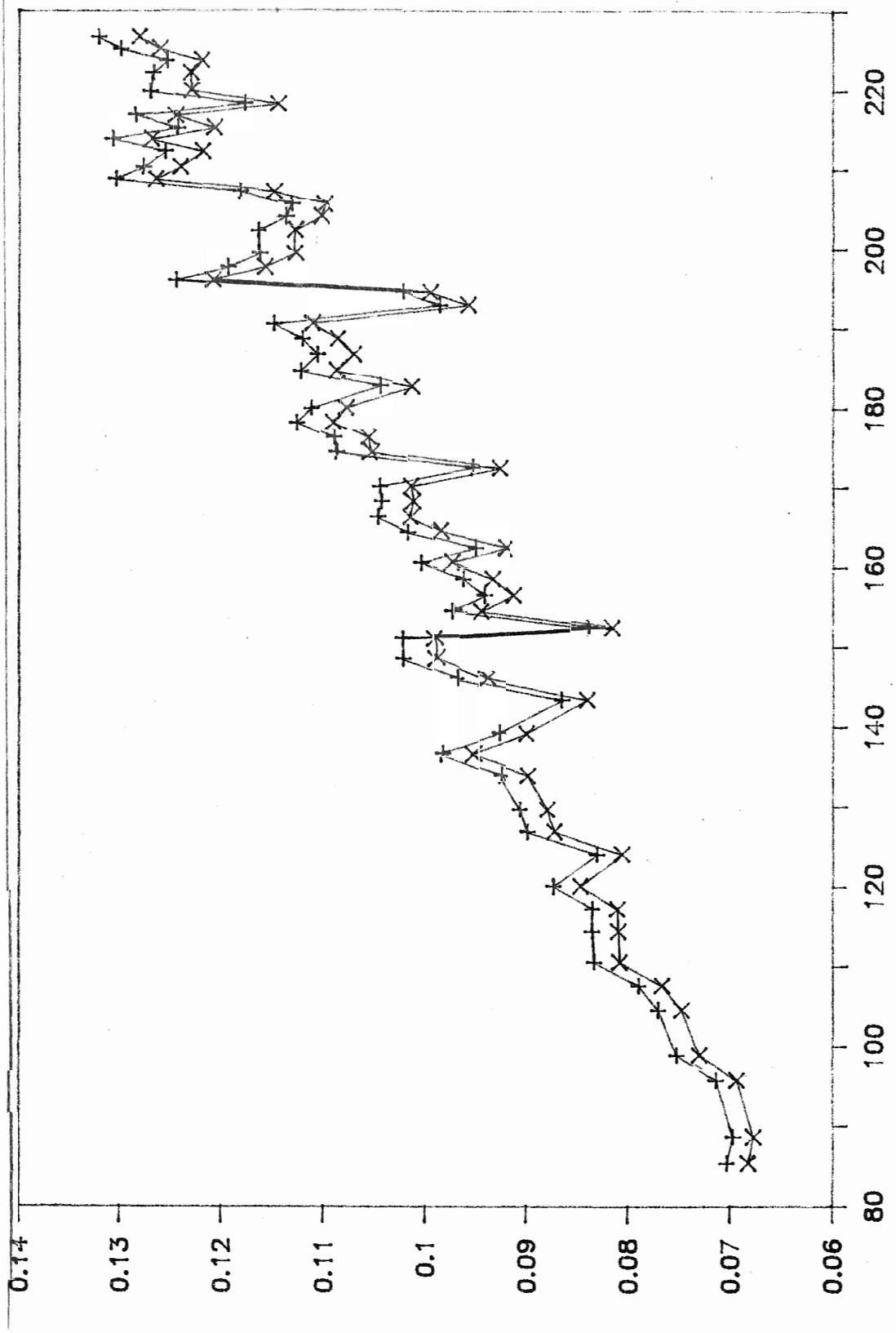
Heat Cap. (J/K)
0.14
0.13
0.12
0.11
0.1
0.09
0.08
0.07
0.06
80
100
120
140
160
180
200
220

II.4. Summary and Concluding Remarks

Despite many efforts, the method of Depuydt and Dahlberg [1] could not be reproduced with this apparatus. A paper search found that these authors had published no further articles using this technique and in fact performed no more heat capacity measurements to my knowledge. Furthermore Dr. Razavi learned from a colleague in Germany that this method would not work.

The calculation for the heat capacity is very sensitive to the final or so called stability temperature at the end of each heating step. This can be seen by noting that the heat capacity is proportional to the difference of two large areas in the graph defined by KT vs t. Both areas are defined critically by the final temperature. One area is evaluated by the integral and the second is a rectangle defined by the final temperature and the duration of the heat step. The existence and successful detection of $dT/dt \cong 0$ becomes critical as this condition defines the final temperature. More importantly, the analysis itself requires that dT/dt be sufficiently close to zero so that the estimate of the thermal conductance is valid. Also the value of the final temperatures of two steps dictate the thermal conductance used in the calculation of the integral. These factors clearly compound and therefore seriously affect the heat capacity calculation.

The question then is, can we actually accurately determine the

final temperature? This is likely impossible since without perfect isolation the sample temperature will always tend to drift. An adiabatic approach with this method cannot be used because the analysis requires a difference in temperature between the sample and bath, exactly what an adiabatic calorimeter is designed to eliminate.

Section III: Sweep Method

The method discussed in the previous section had proven unacceptable, it was therefore necessary to investigate other methods. The short time remaining (four months) meant that a simple technique which was compatible with the equipment at hand was the only option. Investigation of a variety of methods indicated that the Continuous Heating or Sweep Method seemed to satisfy these requirements. This section pertains to the theory, development and analysis of this method of measuring heat capacity.

III.1. Theory of Measurement

As found in the previous section the single largest obstacle to measuring the heat capacity accurately is the unavoidable presence of thermal links to the sample's environment. In fact the various methods that have been developed over the years for low temperature heat capacity measurements are the result of new endeavors to somehow compute or circumvent the effects of the thermal link. The continuous heating method of Junod [2] uses knowledge of a second set of data to avoid computing these heat losses.

The diffusion equation (II.1) can also be written

$$P + dQ/dt = C\, dT/dt , \qquad \text{(III.1)}$$

where dQ/dt is the rate of heat exchange with the environment. Many methods attempt to construct the so called adiabatic calorimeter by placing the sample in a thermally shielding

vessel. The vessel and/or sample temperature is then well controlled in such a way that the difference in temperature between the sample and shield is very small. If the calorimeter were truly adiabatic $dQ/dt = 0$ and the heat capacity calculation is straight forward. However in practise this is not possible and some errors are introduced by believing this assumption true.

Junod's [2] approach was to consider as well the diffusion equation with no power supplied to the sample. The thermal link is still the same and therefore the heat exchange is also equal under the two conditions, P=0 and P≠0. As well, provided the sample characteristics are stable, (always required for heat capacity measurements due to long time scales) the heat capacity as a function of temperature remains the same. Therefore when the power is zero III.1 becomes

$$dQ/dt = C\, dT_o/dt \qquad \text{(III.2)}$$

where dT_o/dt is the drift in temperature when P=0. Substitution into the second form of the diffusion equation (III.1) shows that if this base line drift is measured the heat capacity can be computed by,

$$C = P\, \{dT/dt - dT_o/dt\}^{-1}. \qquad \text{(III.3)}$$

Noting that the sample heater's resistance will change over a large temperature range and of course so will the rates, the heat capacity as a function of temperature can then be more accurately determined if P and the rates are determined as functions of temperature as well.

III.2. Method

In Junod's [2] implementation a temperature control circuit was built to make the shield temperature follow the sample's temporal evolution. This provided sample environment control to produce near adiabatic conditions. This regulation loop then guarantees that the heat exchange with the environment is small compared with the Joule heat supplied to the sample ($dQ/dt \ll P$).

Junod's [2] sample cell was very similar to the one used here (section I, design 2) thus modifications were not made. However Junod's [2] acquisition system was entirely analog. A analog PID (Proportional Integral and Derivative) temperature control circuit regulated the shield temperature according to the difference between the sample and shield temperatures. The sample's thermometer voltage was also input into an analog differentiater the output of which was then plotted as a function of the thermometer voltage on a chart recorder. That is if the thermometer's response function is $f(T)$, then $df(T)/dT \times dT/dt$ was plotted versus $f(T)$. This plot is then proportional to $1/C(T)$.

A straight forward computerization of Junod's [2] apparatus can be achieved by recording thermometer voltage and the analog differentiater output voltage with a computer. Then using the sensors calibration data, compute actual temperature and time rate of change of temperature. Finally using a pre-recorded base line drift compute heat capacity directly using equation III.3.

However the equipment here is almost entirely digital and time would not allow the construction and refinement of the analog circuitry. The approach then is to use the existing temperature controllers to regulate the bath and shield temperatures so that they follow the sample temperature. Feedback is performed by continuously reading the sample temperature and providing this temperature to the controllers as their next set point values. If the PID parameters are appropriately set and communication rapid enough, this software loop maintains a difference in bath and sample temperatures of less then 1%.

The computer program is discussed in appendix E [12e] but a short account is provided here for convenience. The computer program first obtains the temperature range of the experiment requesting the initial and final temperatures. The program also requests the tolerance for stability condition, the power to be supplied to the sample and the output file name for the recorded data. The computer then sets the set point temperatures of both controllers to the initial temperature (which must be less than the final temperature) and waits until the sample, bath and shield temperatures lie within the window defined by the tolerance. Once the system is taken as stable, power is supplied to the sample and data continuously recorded. It is here that the various attempts of this method differ and is therefore left to the next sub-section for discussion.

Once we have a working algorithm the approach is to perform four separate experiments. First collect data without the sample for both the temperature evolution without power supplied to the mount and the again with power applied. From this data compute the rates with and without power and extract the total heat capacity of the mount and all materials present on the mount. Then perform the two experiments again with a sample mounted. The difference of the two heat capacities is the contribution to the total heat capacity due to the sample.

After several experiments have been performed without the sample an average heat capacity can be used, provided the reproducibility is sufficiently high such that the errors are small compared to the sample's heat capacity. The same mount sheet and thermometer are always used, therefore the only materials that change from one experiment to the next are the varnish and sample. Thus, if the contribution to the heat capacity due to the varnish is relatively large, individual runs must be performed. To best regulate the contribution due to the varnish, an experiment without the sample can be performed first. Then the varnish can be softened with some acetone or alcohol and the sample pressed into place. This would ensure that the amount of varnish remains approximately constant over the four separate experiments. However for this method to work, a very thin layer of varnish must be used to ensure good thermal contact.

III.3, Experiments, Results and Discussions

The first step was to choose a numerical method for computing the derivative. While working on the heat step technique the idea of using an non-linear interpolation technique was considered for improved accuracy in temperature measurements, especially for sensors with response functions similar to diodes. The numerical method considered was that of divided differences [9]. This method interpolates assuming an n^{th} degree polynomial fit through locally occurring data. Actually the method can be applied over any range by simply skipping over intermediate values. However the routines written were designed to perform the calculation with local data. This method proved to work very well with third degree fits agreeing within 0.03% of data generated using a fifth degree polynomial. Theoretically the degree used for the interpolation is unlimited, but the time required to interpolate a point increases rapidly with degree chosen [12d]. A major benefit of this technique is that the data set representing the abscissa need not be equally spaced allowing greater leeway in the data acquisition method.

Before use, both the polynomial and derivative interpolation routines were tested by first computing a set of data, stored in a pair of arrays, and then using these data and the routines to interpolate the function and the derivative. These interpolated points are then compared with values computed directly using the generating function and its derivative. Table III.1 and III.2 lists interpolated polynomial and derivative results

representative of these calculations. Table III.1 shows interpolated data assuming a third and second degree polynomial computed from data generated using the function,

$$y(x) = x^3 - 3x^2 + 2x + 3. \qquad \text{(III.4)}$$

The x data given to the interpolation routines are generated such that they lie randomly between any two adjacent x values in the arrays. This guarantees the values are actually interpolated values. The routine does recognize values in the arrays. That is, if the value of x given to the routine is in the x-array then the y-array element corresponding to this x value is returned and no divided differences are computed. For this particular data set the x array contains elements at equal intervals of 0.05.

The generating function of table III.1 (eq. III.4) has two extrema located at $x \simeq 0.423$ and at $x \simeq 1.577$. The third degree results indicate an error of 0% for these, since to the number of digits reported by the computer, the interpolated values are exactly equal to the true value.

Table III.1
Representative Polynomial Interpolations

x	y				
	True	Interpolated Assuming		Percentage Error	
		2nd deg.	3rd deg.	2nd deg.	3rd deg.
0.015	3.029328	3.029284	3.029328	-0.0015	0.0
0.423	3.3849	3.384945	3.3849	0.0013	0.0
1.025	2.975016	2.975063	2.975016	0.0015	0.0
1.54	2.617464	2.6175	2.617464	0.0014	0.0
1.577	2.6151	2.615148	2.6151	0.0018	0.0
2.515	4.962266	4.962301	4.962266	0.0007	0.0
3.05	9.565125	9.565125	9.565125	0.0	0.0
4.01	27.26091	27.26093	27.26091	0.00009	0.0

Table III.2 contains data for interpolated derivatives assuming second and third degree polynomials using the generating function,

$$y(x) = 1 - e^{-x/50}. \qquad \text{(III.5)}$$

For this data, unlike table III.1, the derivatives are computed at abcsissa corresponding to the elements in the x-array. This was done since in the application for this research the derivative is to be calculated at the temperatures recorded. Also contrary to the interpolation routine, there is no array which already contains the derivatives, therefore all values must computed. Due the size of the numbers only the true value and the percentage errors are given in table III.2.

A very sharp Gaussian was also used to test the derivative calculation with similar results. See appendix D [12d] for further details on these interpolation programs.

Table III.2
Representative Derivative Interpolations

x	y'		
	True	Percentage Error (%)	
		2nd deg.	3rd deg.
	($\times 10^{-2}$)	($\times 10^{-2}$)	($\times 10^{-4}$)
10	1.637462	2.7	5.3
30	1.097623	2.7	5.2
70	4.931939	2.7	7.6
110	2.216063	2.7	10
130	1.485472	2.7	13
170	0.6674654	2.7	25
190	0.4474154	2.5	29

The first experiment was only intended to show that the algorithm was functional. Therefore this routine recorded temperatures in the data file at chosen temperature intervals only for later inspection. The first set of data (fig. III.1) showed some degree of fluctuations and some divergence near the end points. However the temporal response is smooth and shows no undesirable behavior (fig. III.2). Digital resolution of the sample temperature is also a factor when trying to compute the derivative. Since this first method used no averaging the derivative was calculated using the last 4 data points (ie. third degree polynomial). This means that as the temperature approaches a temperature at which the reported value will be at the next digital level, the derivative will rapidly increase to a very large value. Conversely when several readings have been at the same digital level the derivative will be zero (figure III.3(a)). It was believed that this was the single largest contributions to the fluctuations in the derivative. Some averaging will break down the digitalization making the data appear continuous.

Since the program did not record the data continuously, recall that the program records the data only when $\Delta T \geq$ some preset value, many data points were simply unused. Therefore the next approach was to use all the data so that the stored values actually represented a local average in temperature and time. Note that as long as the temporal evolution is nearly linear then an average time is acceptable, however if the response is not

Figure III.1, Initial Data

Plot of time rate of change of temperature as a function of temperature.

Figure III.2, Temporal Response

Temperature vs time data using continuous heating software feedback method.

Figure III.1

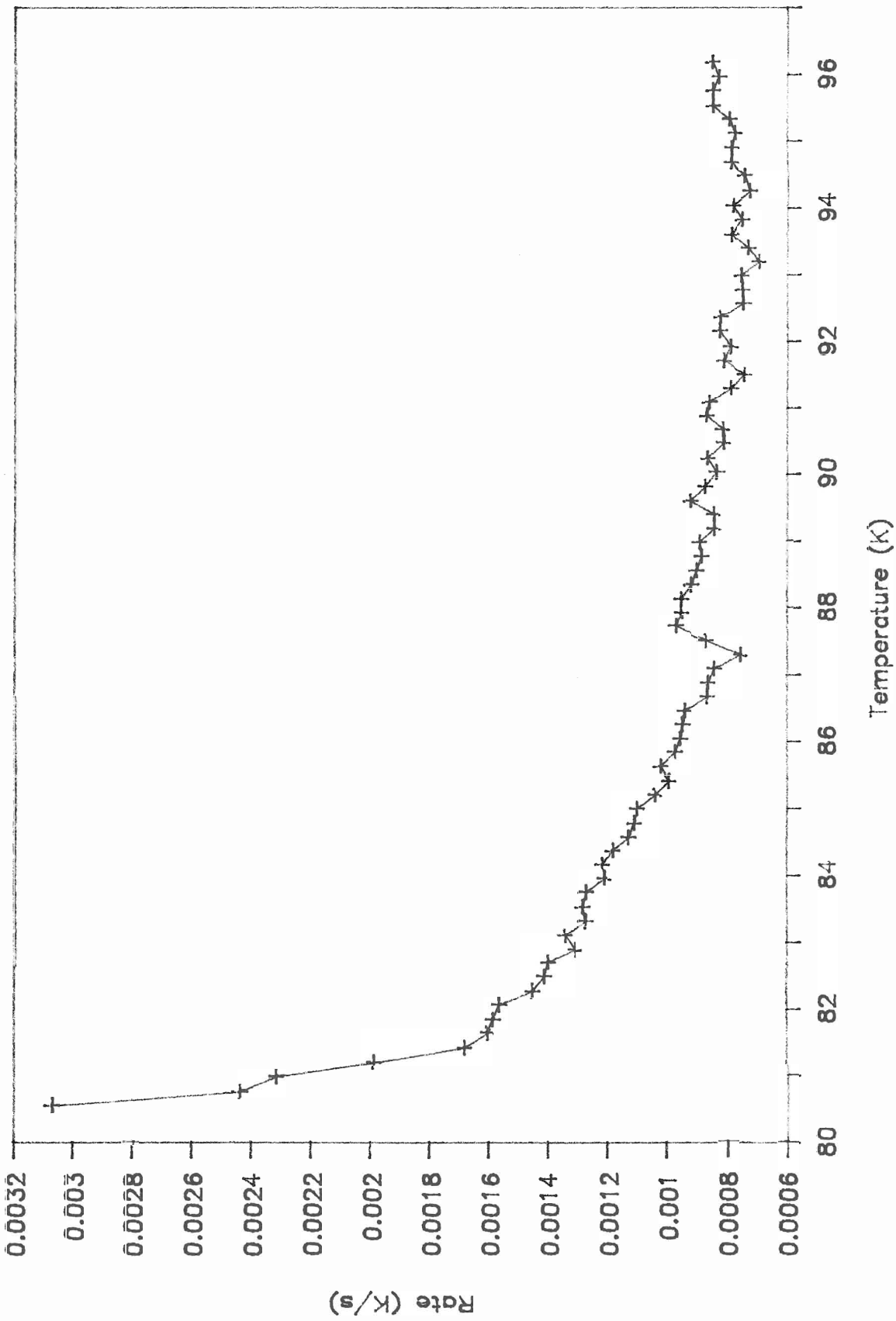
0.0032
0.003
0.0028
0.0026
0.0024
0.0022
0.002
0.0018
0.0016
0.0014
0.0012
0.001
0.0008
0.0006
Rate (K/s)
80
82
84
86
88
90
92
94
96
Temperature (K)

Figure III.2

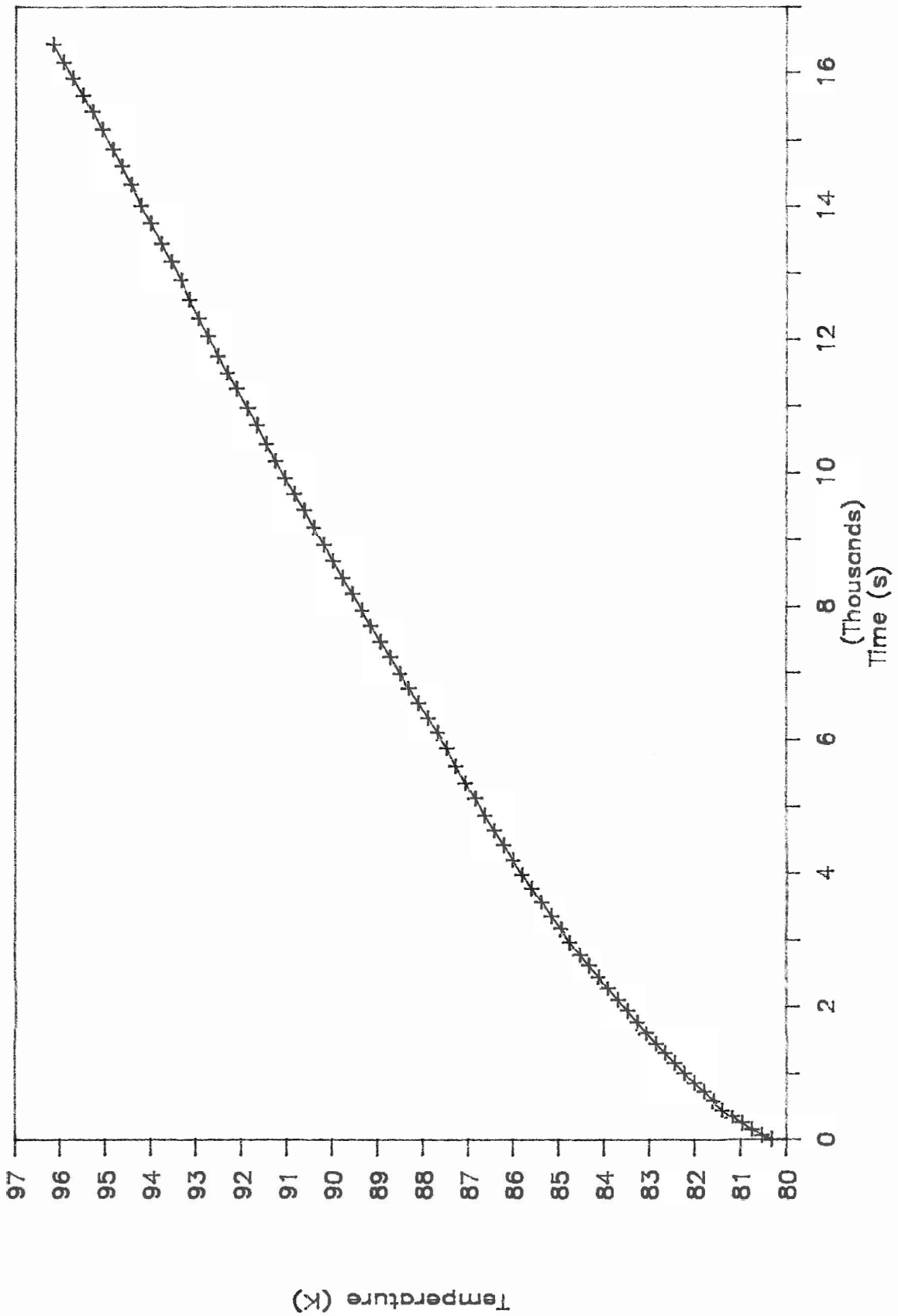
Temperature (K)
97
96
95
94
93
92
91
90
89
88
87
86
85
84
83
82
81
80
0
2
4
6
8
10
12
14
16
(Thousands)
Time (s)

sufficiently linear, then the average time and temperature are not a properly matched data pair. That is the average temperature will not have occurred at the average time.

The simplest method would be to use some number of points before and after the temperature at which a data set are to be recorded, to compute averages and store these values. However if a window type of averaging is used then there is less chance of skipping over any important data. This approach will also allow the rate to be continuously displayed while the experiment is in progress. Also if all the other required data has been obtained, a continuous display of the sample's heat capacity can be provided. A window or moving average always uses n points to compute the average but rather than each time skipping n at a time, each individual value is used n times to compute n separate averages as the window moves through the data set one point at a time.

The program must therefore perform two tasks, one is to somehow maintain the moving averages, the other is to compute the derivative. Two different methods were considered and differ only in the order in which these tasks are performed. The first method first computes the moving averages and then stores these in separate arrays for use in the derivative routine to calculate the derivative of the average time rate of change of average temperature (ie. d<T>/d<t>). The second computes derivatives first using the raw data and then reports the average of n derivatives (ie. <dT/dt>).

Figure III.3, Problems With Derivative Calculation

(a) Illustrates the affect of digitalization on derivative calculation. The solid line represents the actual temporal response. The dots are the digitalized data points. The dashed lines represent approximate slopes fitted through 4 points at a time.

(b) Effect of local high order fits to data with scatter. The solid line represents actual response. The dots are the scattered data points. The dashed curve represents the fitted curve using the four points (ie. third degree). The straight line segments are the computed slopes at the data points.

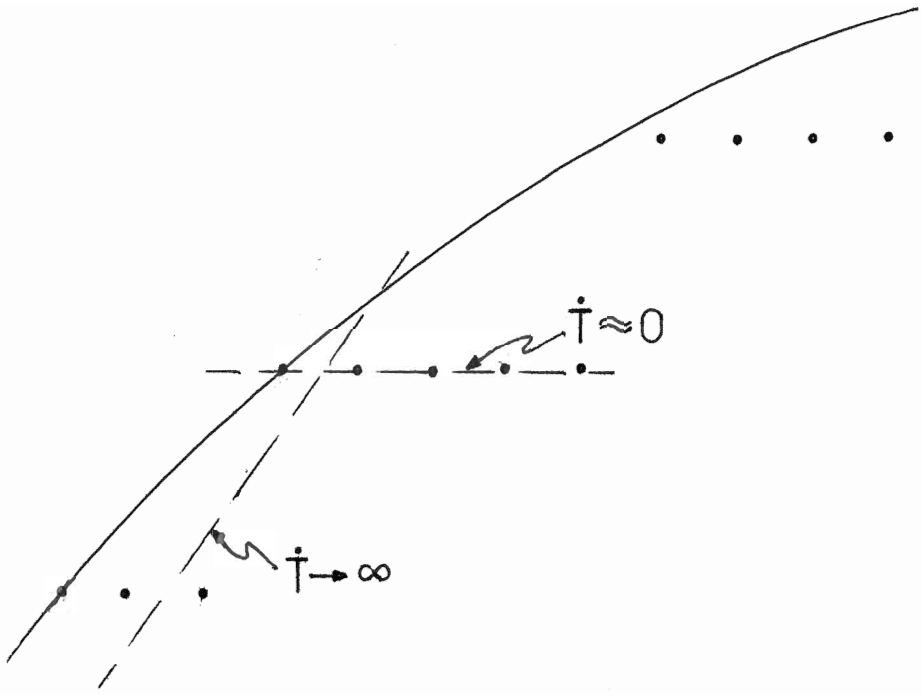

(a)

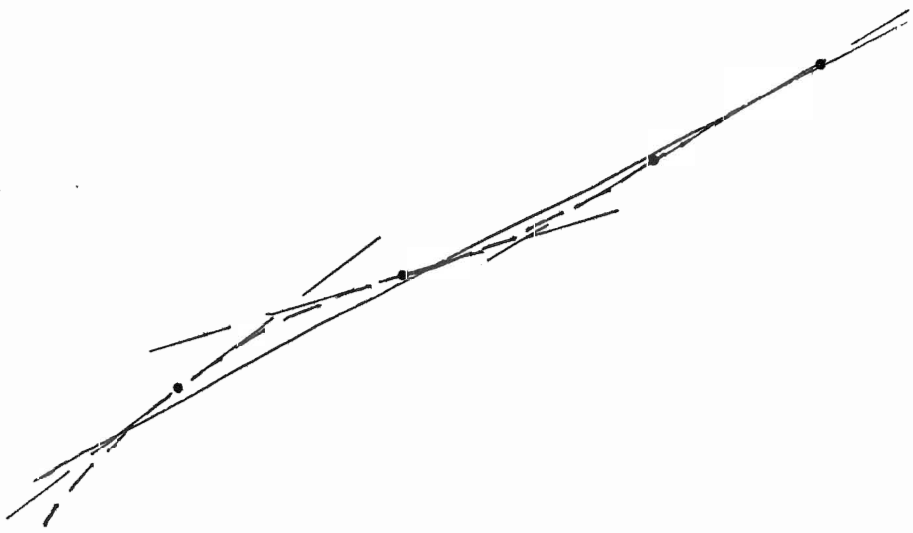

(b)

Figure III.3

To test the system the actual heat capacity was not evaluated since this requires four experiments. Instead the results of a single run with the sample and mount shall be referred to as the pseudo heat capacity,

$$C' \equiv P \ (dT/dt)^{-1} \ . \qquad \text{(III.6)}$$

This result is dimensionally correct but represents the uncorrected total heat capacity of the sample and mount. This result is also exactly what is used for a truly adiabatic calorimeter. This data should however give some idea of the performance of the method and the heat capacity to an order of magnitude.

The first measurements obtained by these methods showed little difference in the two methods but did imply somewhat, that the first of these two methods provided slightly smoother results. However fluctuations in the pseudo heat capacity still remain. Experiments were performed with the number of points averaged equal to 5, 10, 15 and 20. The magnitude of the fluctuations were reduced with each subsequent increase in the averaging number but still persisted at a magnitude greater than desired.

The degree of the polynomial is also adjustable, the higher the degree, the greater the number of points used to compute the derivative. However it turned out that with increasing the degree from 3 to 4, the magnitude of the fluctuations actually increased and using a second degree polynomial produced a very smooth curve for the pseudo heat capacity. Apparently the higher

degree fits attempt to fit a rapidly varying function to the locally occurring, slightly scattered data. As a result the computed derivative shows large fluctuations as the slopes can then be rapidly varying (see figure III.3(b)). All the results obtained using the second degree polynomial demonstrated a smooth promising response. Figures III.4 to III.6 are results of several independent experiments.

To compare these results to accepted values, the heat capacity of the sample itself must be evaluated by performing the additional experiments outlined earlier. However it became necessary to pursue a third technique to facilitate low temperature (< 40K) measurements (see next section). It was believed that the pseudo heat capacity would reasonably approximate the total heat capacity of the sample and mount sheet since the equation for the pseudo heat capacity (III.6) is the same as for a truly adiabatic calorimeter. Also the contributions from the GE varnish, solder and thermometer element are believed to be small compared to the total mass of the of the copper sample and mount sheet.

Figures III.4 - III.6 illustrate the performance of the apparatus. Figure III.4 shows the temporal response of the sample. The data is smooth and well resolved and the problems associated with digital resolution have been reduced by the averaging technique. Figure III.5(a) shows sample temperature versus bath temperature and the straight line represents the line

Figures III.4-III.6, Apparatus Performance

Figure III.4, Temporal Response

Temperature as a function of
time elapsed since power to sample switched on.

Figure III.5, Bath vs Sample Temperatures

Graphs illustrate effectiveness of feedback mechanism, bath temperature should follow sample temperature.

(a) Plot of bath temperature as a function of sample temperature. The straight line represents the line y=x.

(b) Plot of relative error of bath temperature from sample temperature as a function of time.

Figure III.6, Stability of Heater Power

Graph of power as a function of sample temperature.

Figure III.4

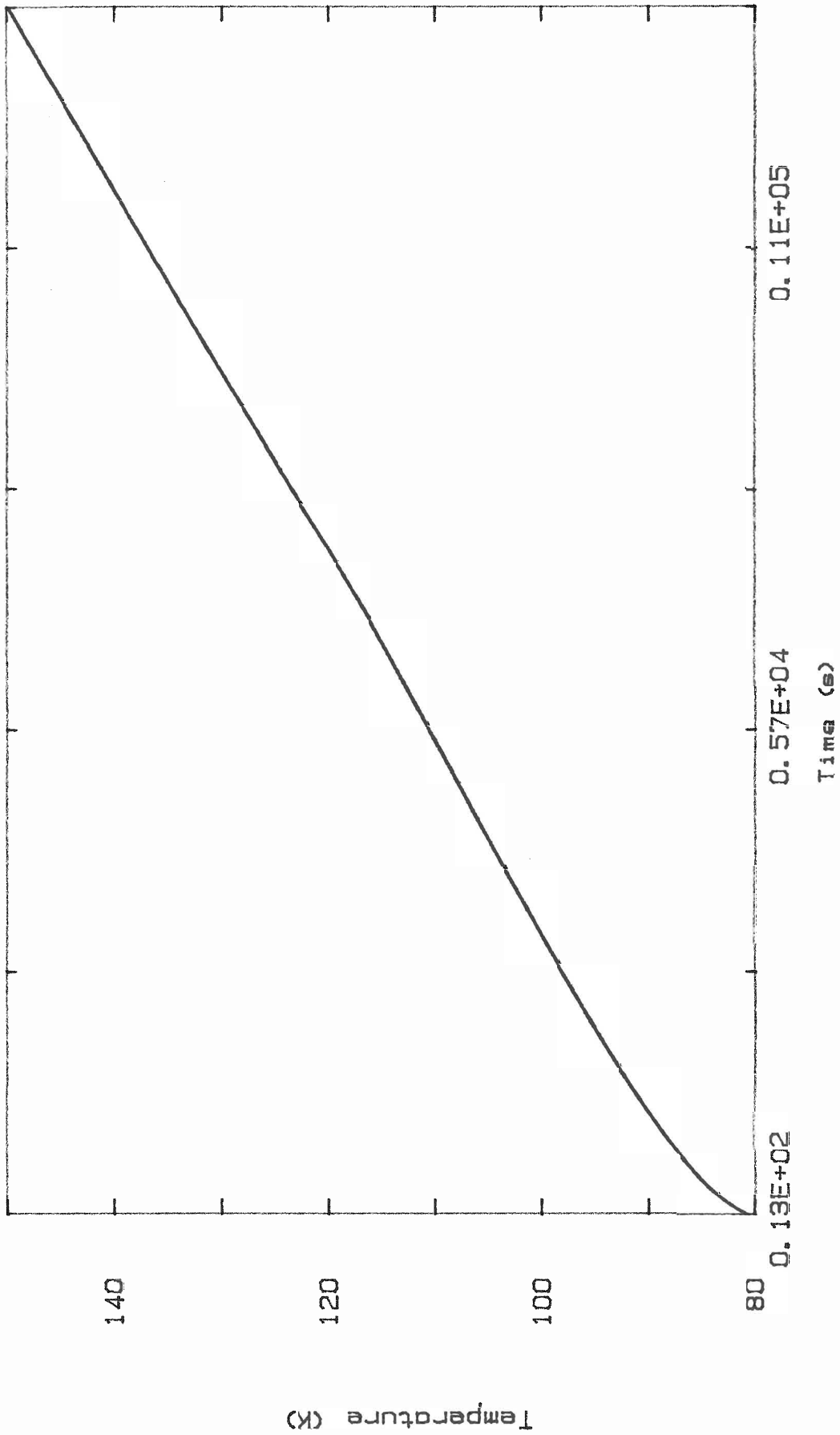

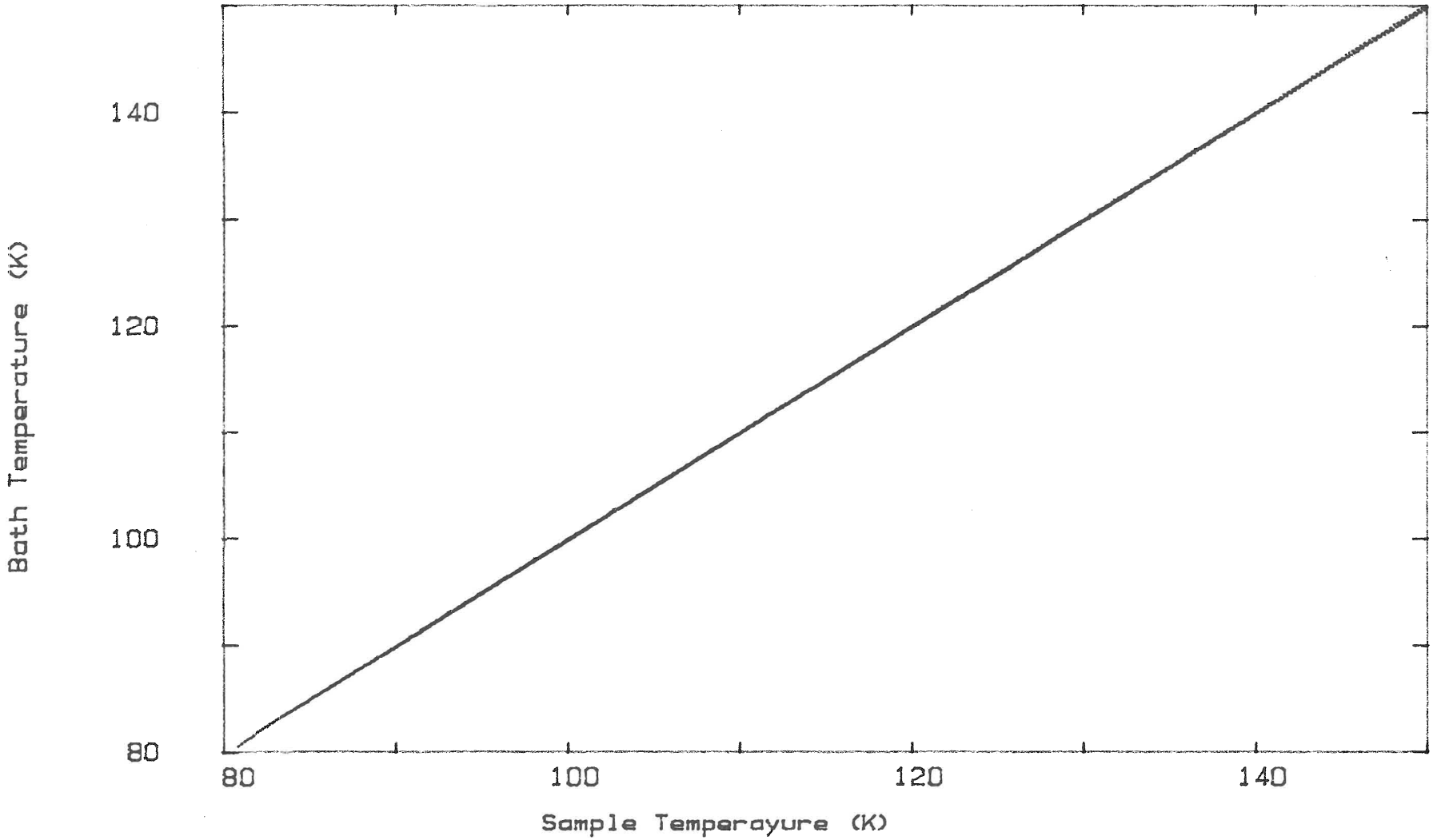

Figure III.5(a)

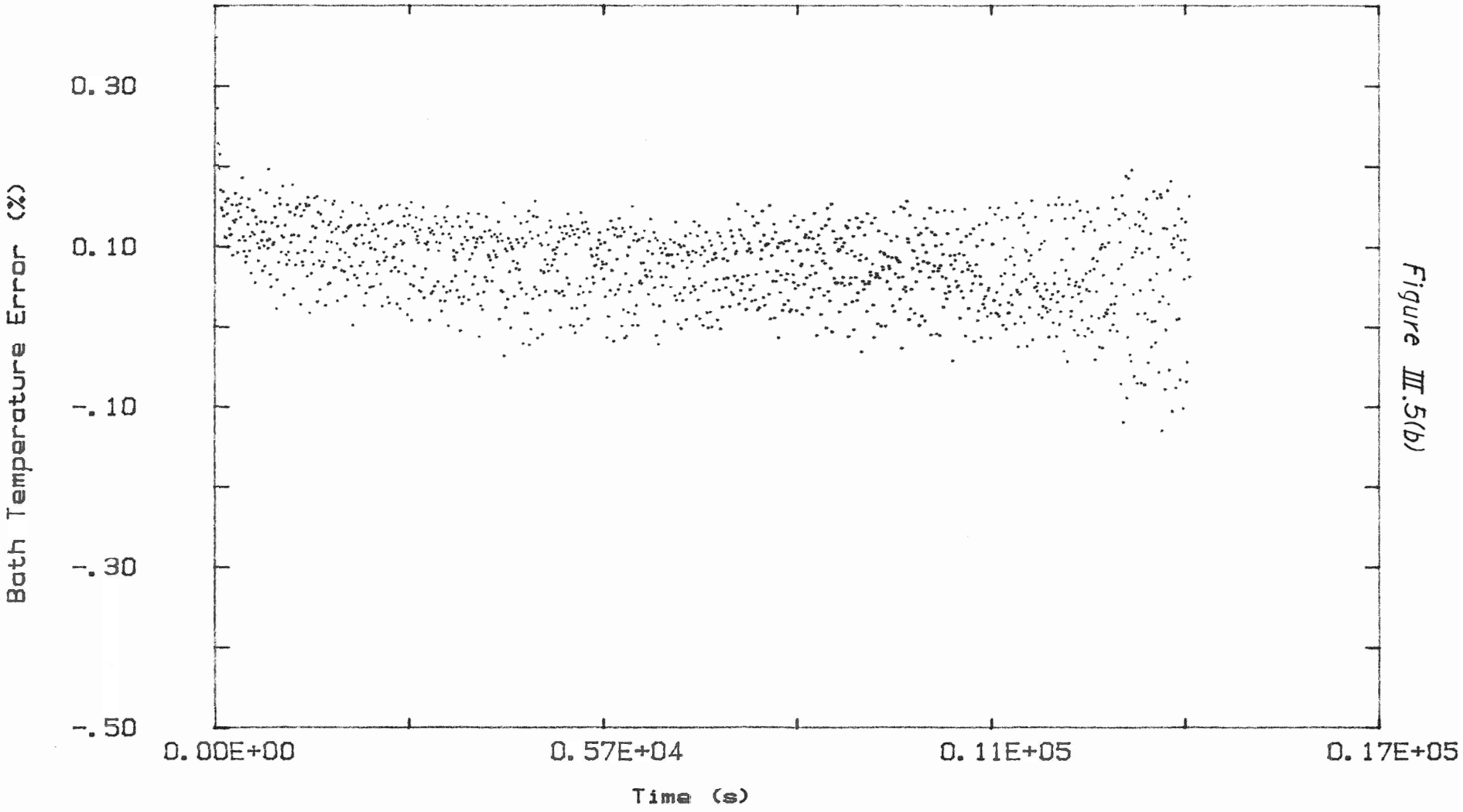

Figure III.5(b)

Figure III.6

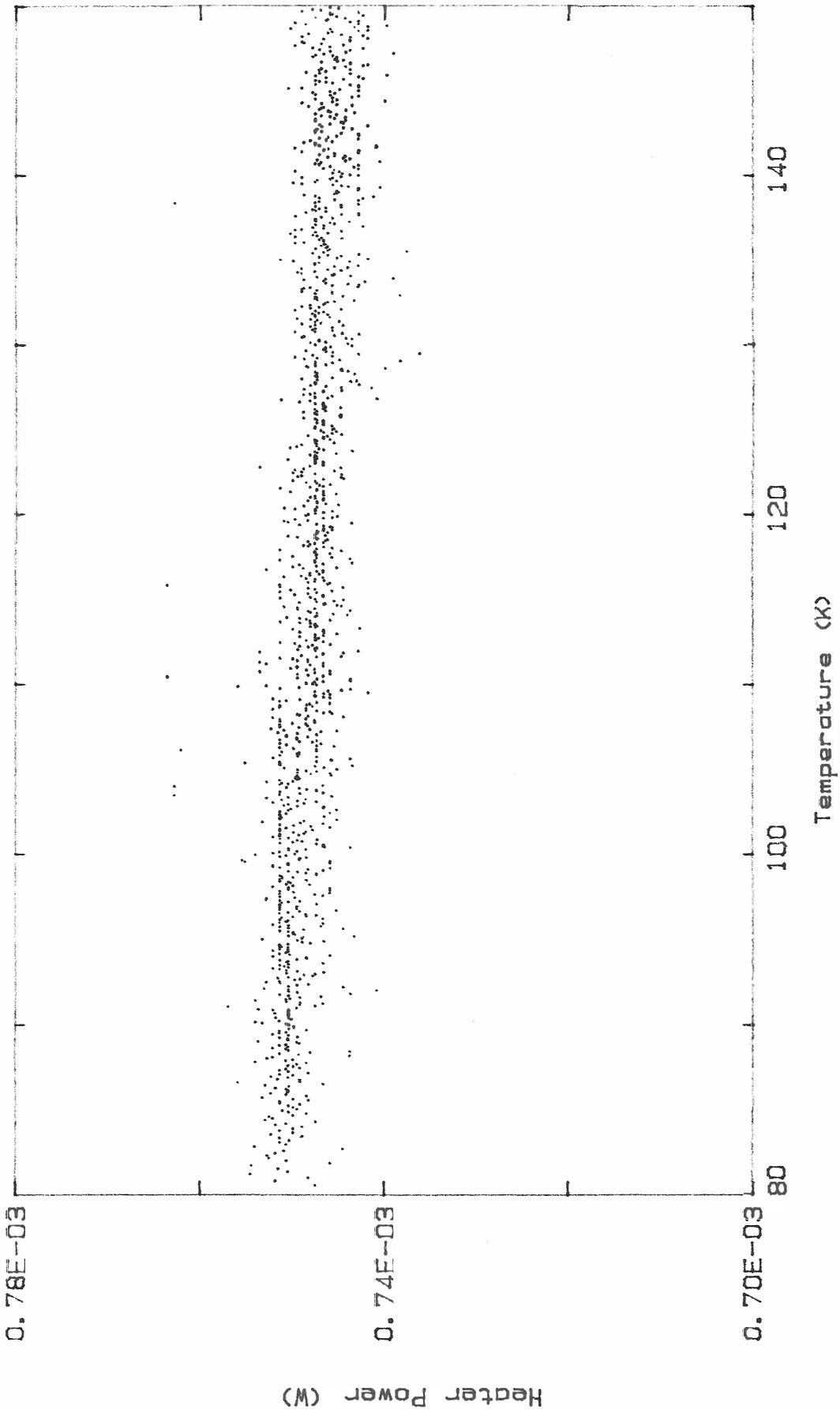
0.78E-03
0.74E-03
0.70E-03
Heater Power (W)
80
100
120
140
Temperature (K)

y=x. Figure III.5(b) gives the error between sample and bath temperature as a function of sample temperature, that is $\delta T(T)$. Figure III.6 indicates the stability of the power supplied to the sample by plotting power versus time. The scatter is only in the order of 1% with fluctuations in power of $\sim$0.001mW.

Figures III.7-9 shows the pseudo heat capacity results for three independent runs. A comparison of III.7 and III.8 indicates that the results at least appear reproducible since the shapes are comparable and the ranges approximately the same. A comparison of these with III.9 shows disturbing similarity in the range of values for heat capacity, despite the different temperature ranges. However recall that these are the pseudo heat capacities and that the full set of measurements introduces a further dependence of the environment by using the base line drift to account for heat exchange with the environment.

Figure III.10 is a plot of heat capacity versus temperature from accepted values for copper assuming that the dominant contributions to heat capacity are from the copper sample (47.17 ± 0.01mg) and the OFHC copper mount sheet (51.51 ± 0.01mg) constituting a total mass of 98.68 ± 0.02 mg. A comparison with experimental data can only indicate agreement to an order of magnitude since the secondary contributions to the heat capacity from the; solder, GE7031 varnish, strain gauge and electrical leads are not known. A conclusive comparison can only be performed if a complete set of experiments are performed as

Figures III.7 - III.9

All are plots of pseudo heat capacity as a function of sample temperature for three independent runs.

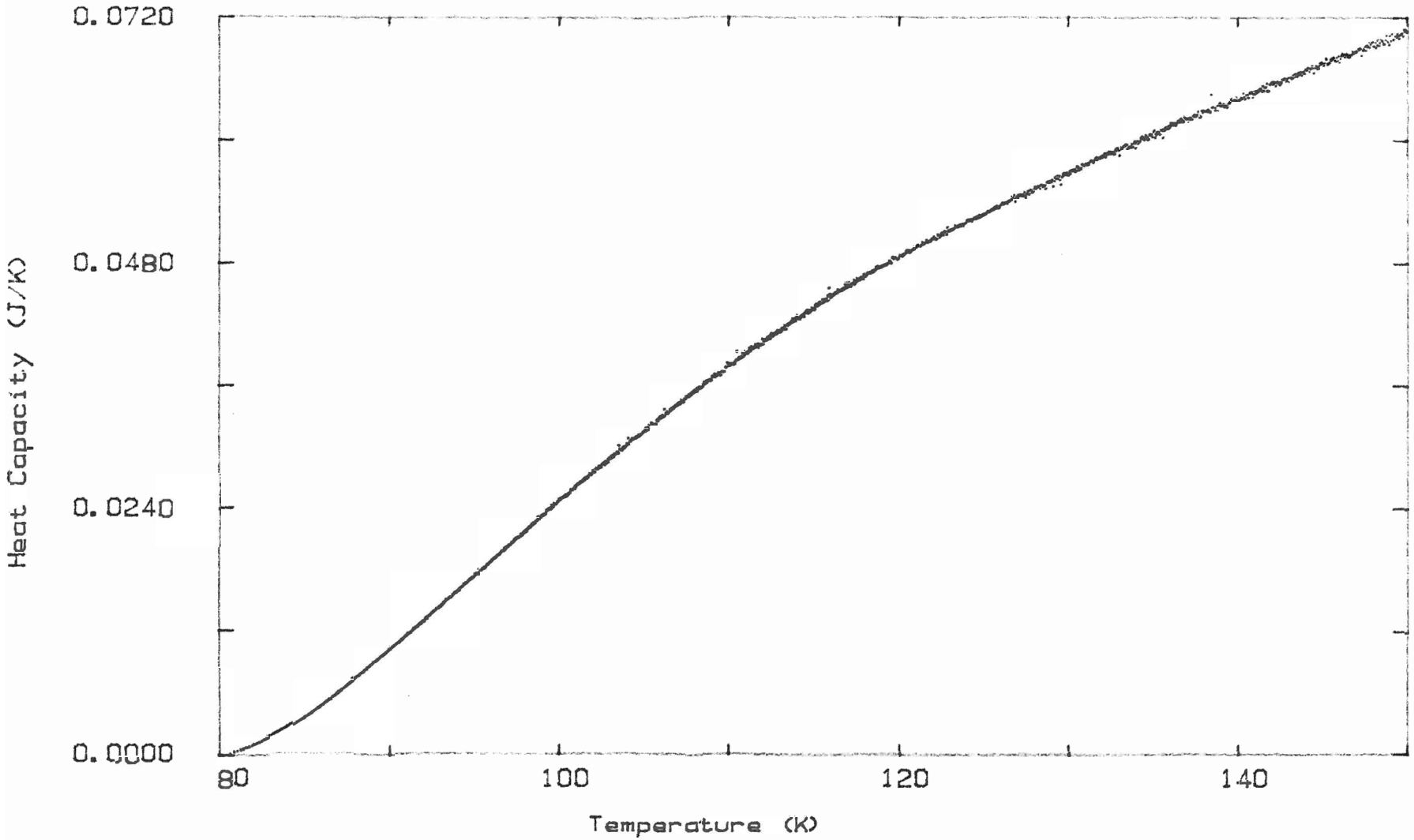
0.0720
0.0480
0.0240
0.0000
Heat Capacity (J/K)
80
100
120
140
Temperature (K)

Figure III.7

Figure III.8

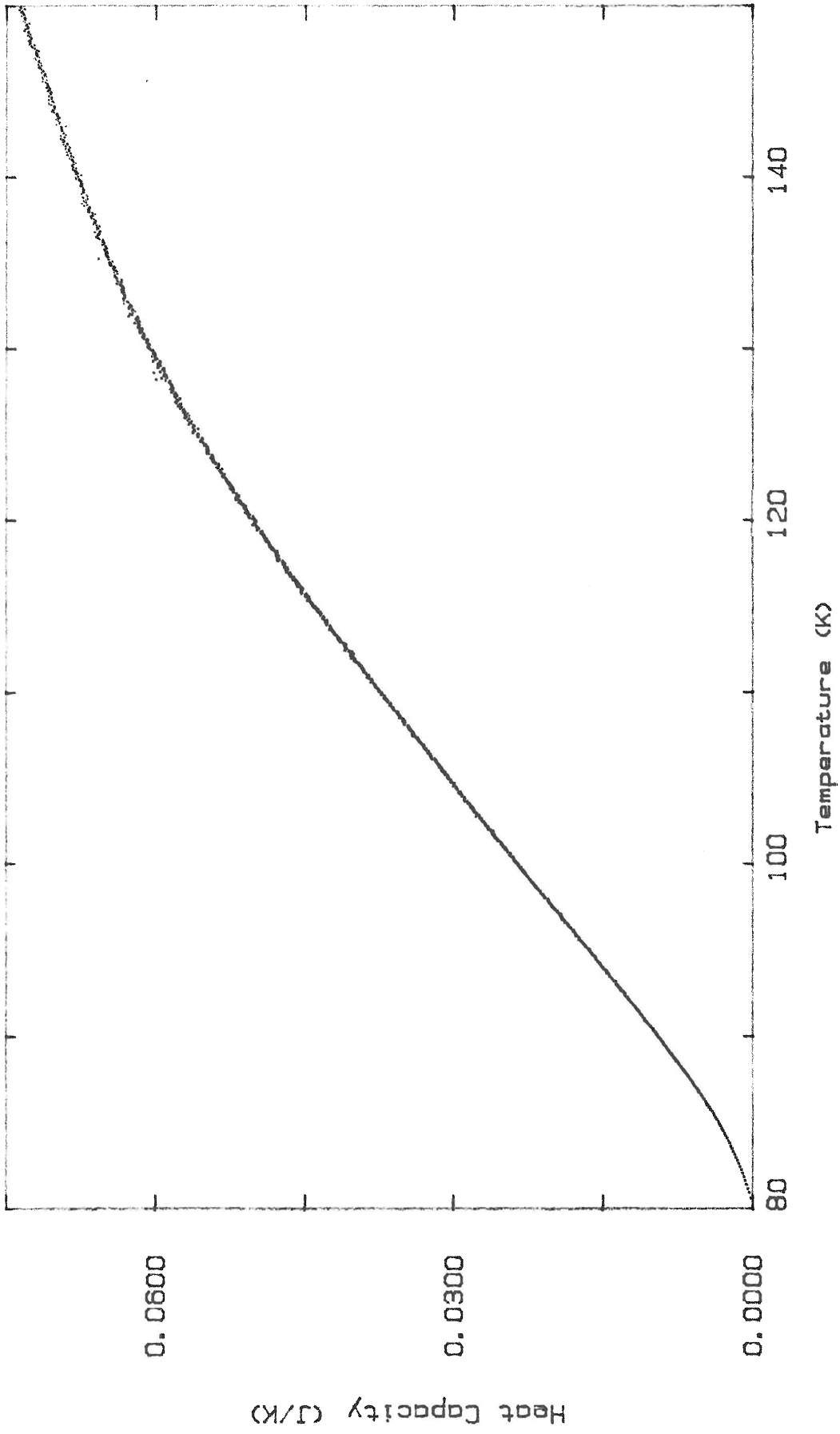
Heat Capacity (J/K)
0.0000
0.0300
0.0600
80
100
120
140
Temperature (K)

Figure III.9

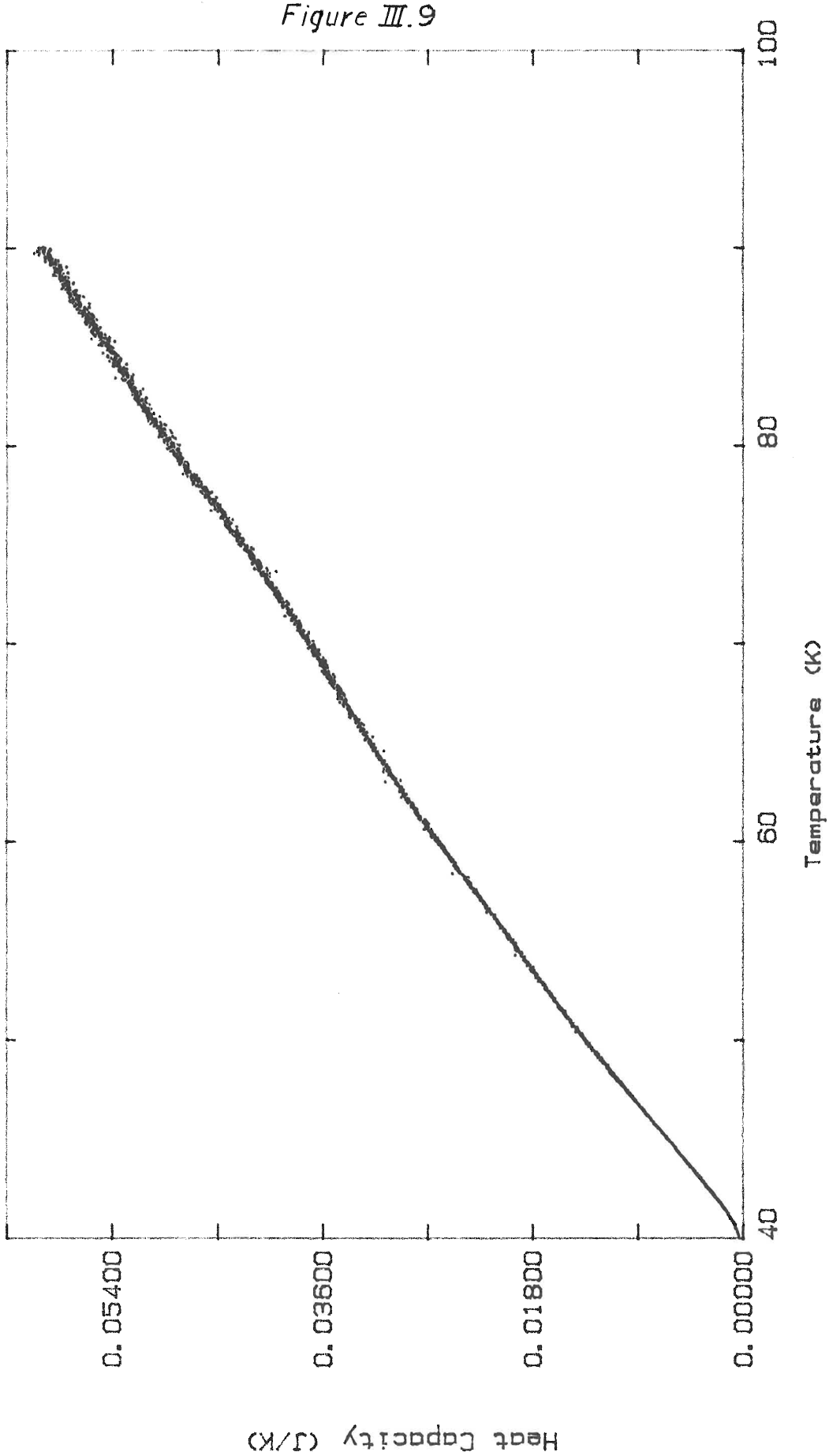
Heat Capacity (J/K)
0.05400
0.03600
0.01800
0.00000
40
60
80
100
Temperature (K)

Figure III.10, Accepted Heat Capacity

Graph of accepted heat capacity as a function of temperature for a copper sample of mass 98.68mg.

Figure III.10

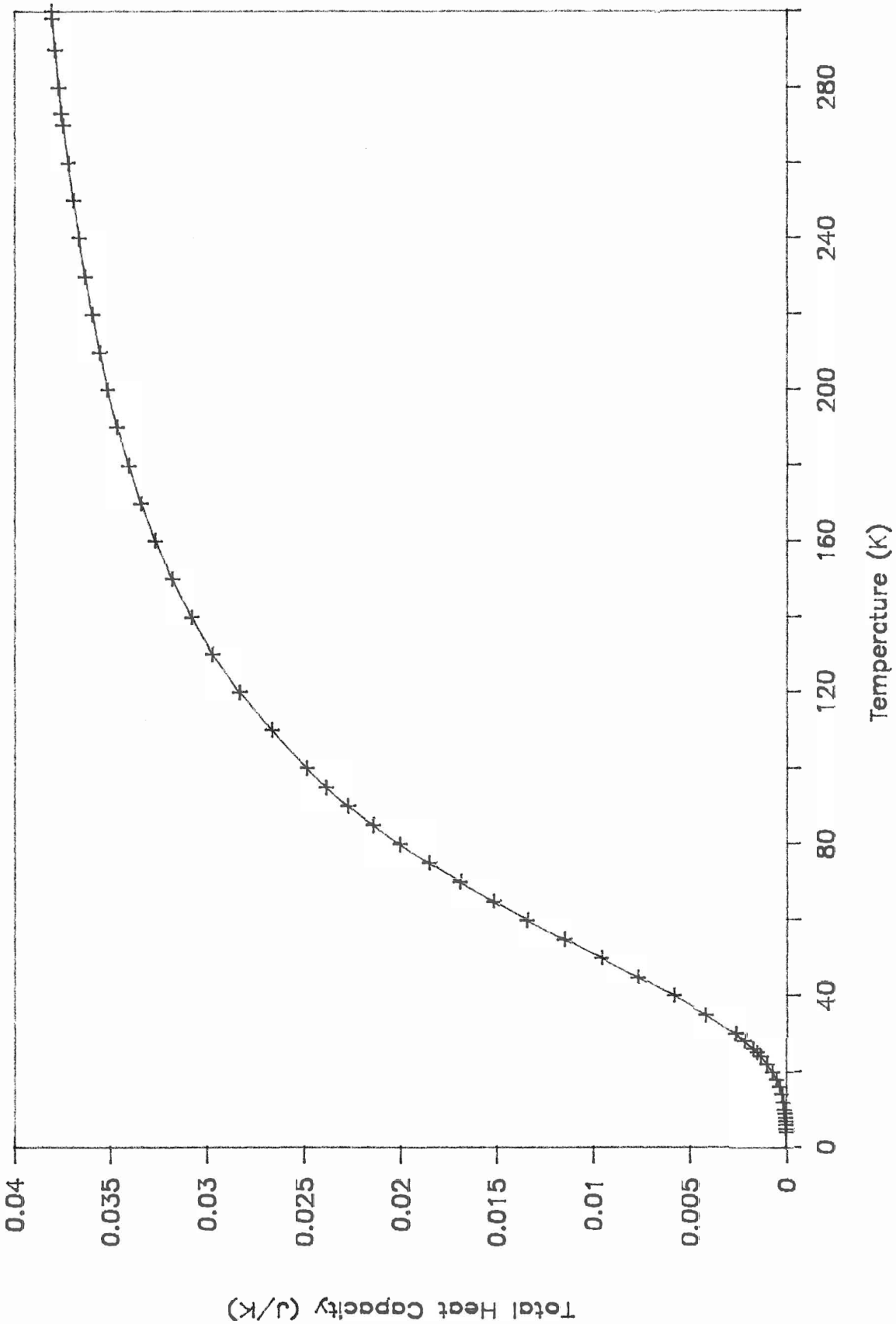

outlined in the procedure to obtain the sample heat capacity. Unfortunately these further measurements were never performed since another method had to be examined for performing low temperature measurements.

All plots of $C_p(T)$ show an initial divergence from the general trend exhibited in the plot. The magnitude of the difference decreased as time progressed. This discrepancy is likely due to the time required for the bath temperature to properly follow the sample temperature. That is when power is first supplied to the sample, the sample temperature increases more rapidly than the combination of the speed of the software control loop and the PID parameters can follow. In time the temperature difference is reduced to the level sustained during the remainder of the experiment (figure III.5(b)). Some experiments also showed some deviation from the trend near the end of the experiment but this is attributed to liquid coolant boil off. This notion is supported by the observed linear temporal response previously observed with coolant boil off when power is supplied to the sample.

Another source of error in the experiment was observed when monitoring the system response to a slightly off-linear-with-time temperature ramp. The actual temporal response observed in the first few experiments, demonstrated a slightly non-linear response at the desired rate of approximately 10mK/s [2]. Therefore a program was written to establish the best PID

parameters for this method by providing set points generated by a slightly off linear function. It continuously displays the sample and bath temperature or shield temperature graphically as functions of time while allowing control of the PID parameters of either controller. It was found that the bath temperature controller could be made to successfully follow the ramp temperature ($\delta T \leq 40mK$) while no combination of PID parameters successfully made the shield temperature follow the ramp using the Series 5500 controller. Examination showed that when a new set point is provided to the Series 5500 controller the power is momentarily shut off or at least reduced even though a higher temperature was introduced. In the continuous heating method set points are continuously fed to the controllers, therefore the heater power never reaches the level required quickly enough. The result is the shield temperature lags further and further behind the sample temperature.

It was also observed that experiments over different temperature ranges (40-70K and 80-150K) showed similar results in the magnitude of heat capacity and the temporal response. These experiments were performed with two different liquid coolants, helium and nitrogen respectively which implies some dependence on the liquid bath temperature. Recall that a full evaluation of the sample heat capacity requires four separate experiments two of which measure the so called base line drift in temperature, dT_o/dt, which will be different for different liquid baths. However the computer algorithm used to measure the drift when

power is supplied to the sample does not work well for the base line drift. When no power is supplied to the sample the drift is small and the derivative calculation produces bad results with high scatter resulting from the resolution. A substantial improvement may be obtained if rather then measuring continuously, one of the original methods is used. Namely record average times and temperatures at larger temperature intervals, say 2 - 5K. Another approach would be to take measurements at temperature intervals or a combination of a temperature interval and a maximum time interval. In any event an accurate measurement of the base line drift is required before the sample heat capacity can be determined.

The problem with the shield control also must be corrected before reproducible results can be attained. Since the problem is believed to be with the Series 5500 controller one solution is to remove this device from the system. A solution is to replace the temperature controller with an analog PID circuit which adjusts heater power according to the difference in temperature between either the sample and the shield or the shield and bath.

The bath control could also be improved so that the temperature more closely follows the sample temperature. With the present technique the bath temperature always lags behind the sample temperature. Attempts using the PID parameters to reduce the temperature difference or to at least cause small oscillations about the sample temperature so that average difference is nearer

zero were unsuccessful. The bath temperature would only lead the sample temperature if large oscillations were set up. Also the average of these oscillations still lagged behind the sample temperature. Therefore, PID values which result in the bath temperature lagging behind the sample temperature with a smooth response were the best that could be obtained. Other PID values caused the temperature to just lag further and further behind.

The fact that with the best PID values the bath temperature lags behind the sample temperature implies that the software feedback loop is too slow. PID control in a sense predicts the temperature through the derivative term, this is part of the success of PID control. The use of a software PID control to predict the next set point rather than use the present bath temperature may improve performance. Another approach would be to use the temperature controller in a different manner than it is designed. The DRC controller has two thermometer inputs, one can be used to measure the sample temperature in the usual manner while the second could be connected in a differential mode where the voltage presented to its inputs is proportional to the temperature difference of the bath and sample. Then by changing the calibration curve used for this input a set point of say 100K could be used which corresponds to zero temperature difference. Implementing the approach is not straight forward, some external circuitry is required, which would need to be designed and tested, again a time consuming endeavor. Note that this sort of scheme could also be used with the other controller which would

immediately eliminate the problem of entering new set points.

As stated earlier, all of these possible solutions have not been attempted due to the limited time remaining. It is hoped that these suggestions will be useful to someone attempting to follow up on this project.

Section IV: The Decay Method

Recall that various alternative methods were considered after the failure of the first method. The methods had to be adaptable to the existing equipment. However none of the methods which satisfy this condition were applicable over the full temperature range and therefore two separate techniques are required. The method of the previous section is applicable above ~40K. This section of the report discusses the successful attempt of the method used below 40K, the decay method of Bachmann et al [3] and Lawless et al [10]. This method is the preferred one of the low temperature methods as it is ideal for observing phase transitions.

IV.1 Theory of Measurement

The solution of the usual diffusion equation (II.1) for heat capacity can also be written,

$$C(T) = (dT/dt)^{-1} \left[P - \int_{T_o}^{T_1} k(T')\, dT' \right], \qquad \text{(IV.1)}$$

where the time dependence of the effective thermal conductance is not explicitly stated, that is the integral is now over temperature not time (there is an implied integration over time since T = T(t)).

To reach a the steady state at temperature T_1, the power required to raise the sample temperature from T_o to T_1 is,

$$P(T_1) = \int_{T_o}^{T_1} k(T')\, dT' , \qquad \text{(IV.2)}$$

where k is the effective thermal conductance of the link. Unlike the modified heat step method of section II, the bath temperature is T_o, while in the modified heat step method the initial temperature of the integral is the starting temperature of the heating step.

The integral of equation IV.2 is the same as in equation IV.1, therefore if one initially measures power as a function of temperature, the heat capacity can be calculated from the temporal response of the sample as it cools from the final temperature. Thus Substitution of IV.2 into IV.1 gives,

$$C(T) = - (dT/dt)^{-1} P(T). \qquad (IV.3)$$

IV.2 Experimental Method

The procedure then is as follows. The sample is initially brought to a thermodynamic equilibrium with its environment. Then, as in section II, the sample is heated by successive heating steps, each reaching as stable as possible state (recall that the sample temperature tends to drift upward). The average power supplied during the heating step and the final temperature reached (also taken as an average of the final 10 readings) for each value of P are recorded. This data is then used in conjunction with the polynomial interpolation routine [12d] to effectively give power as a function of temperature, P(T).

The sample is heated through the small successive heating steps until the desired final temperature is reached. The power is then suddenly shut off and the sample's temperature decays to the

original equilibrium temperature. The temporal response of the decay is recorded and the time derivative of the decay as a function of temperature is computed using the derivative routine [12d]. The rate and power are interpolated at the recorded temperatures to compute the heat capacity at these temperatures.

This method is used for low temperature measurements (< 40K) where thermal radiation is not a problem. Thus the complications of environment control are of no consequence as discussed in the next paragraph. The sample chamber is simply submersed in the liquid helium bath and allowed to cool to its equilibrium temperature. Typically sample temperature of ~5.2K can be reached with this apparatus.

The sample heater (the strain gauge) can readily raise the sample temperature to greater than 40K so that measurements from 40K down can be made without regulating the environment. The measurement is simplified and helium consumption greatly reduced since bath and shield heaters are not required and the sample is well isolated from the liquid bath. The computer program used is a modified version of the modified heat step program. Therefore decays to different environment temperatures can be performed by using the controllers to maintain a steady environment temperature. This procedure may help to examine a transitional region in more detail since the decay rate will be reduced by bringing the environment temperature to just below the transition temperature. Also the extensive program written for section II

can still be used.

IV.3 Results and Discussion

If the rate is high then the experiment is too short to obtain a sufficiently large amount of data for accurate and detailed results. On the other hand if the rate is very slow then the experimental resolution and small fluctuations in temperature create large errors in the derivative calculation and therefore the heat capacity. The ideal rate can only be determined through experiment and experience but a transition free 15K decay in approximately 2000 seconds as performed by Lawless et al [10], was taken as a target. The decay rate is proportional to the strength of the thermal link and inversely dependent on heat capacity. Therefore to obtain the decay rate desired with samples of small heat capacity (ie. small samples or those with small specific heat), it is particularly critical that the thermal link to the bath be weak.

The first experiment was performed without modification to the calorimeter in the temperature range 15 - 20K. The stability condition constraint of section II was loosened to 0.0015 to shorten experiment duration. Nonetheless, the heating steps were well behaved and produced a smooth P(T) curve with the expected parabolic behavior. However the initial portion of the decay was very rapid with the temperature decreasing to ~7k in less then 50s. During the remainder of the decay the rate gradually decreased with sample temperature never reaching the initial set point. However this was not checked using the usual tolerance

window which may explain why the sample appeared to not return to the original equilibrium condition. This experiment provided poor results with the very low rate near 5K providing a large heat capacity. The high rate at the beginning (from 20 down to 7K) provided information at only a few temperatures (~20 points) and rather small values due to the large rate. Finally, although not clear from the temporal data of the decay, a broad hump in the heat capacity data was seen with a centre at approximately 9K.

If we examine the equation for the heat capacity (IV.3) it is clear that the heat capacity can be calculated accurately from the data only until some temperature just greater than the initial equilibrium temperature has been reached. After this point the rate and power reduce to zero or near zero since the sample is approaching the environment temperature, and therefore $C \rightarrow 0/0$.

For the next experiment the strength of the thermal link was reduced by removing the primary thermal link, the no. 30 copper wire. As a check the temporal response of the entire system was monitored on cooling with liquid helium. Soon after liquid helium persisted around the cell, the bath temperature reduced rapidly to liquid helium temperatures (<10 min.). Similarly once the bath temperature was established the shield temperature reduced within 20 - 30 min. to a comparable temperature. The sample however appears well isolated, it generally took several

hours to reach liquid helium temperature from about 70K. Once attained, the temperatures were all very stable, exhibiting no significant drift for large observation times (~ hours).

Despite the apparent low thermal conductance of the link, experiments provided results similar to that discussed above. Once again the decay was too rapid (<< 1hr), and produced a broad hump in the $C_p(T)$ curve.

The proposed explanation for the rapid decay despite the weak thermal link, was that on cooling, the rate is very slow allowing the temperature gradient between the sample and bath temperatures to occur across the entire length of the link at all times. However the sample is heated by the successive heating steps relatively quickly to the starting temperature of the decay. As a result the temperature gradient occurs over only a portion of the link and the remainder is still at the bath temperature (see figure IV.1). This increases the effective thermal conductance of the link by reducing effective length of the link.

To correct for this effect the next experiment was performed with smaller heating steps, (approx. 0.3K) increasing the heating time. This was expected to allow the gradient to exist over most or all of the link. This did improve the decay time but still not comparable to the times demonstrated by Lawless et al [10]. Once again the heat capacity versus temperature data demonstrated a response similar to those observed earlier. Clearly modifications to the calorimeter are necessary.

Figure IV.1, Gradient Problem

Illustration of problem with temperature across thermal link, K. S represents the sample and B the bath. G indicates the region over which the temperature gradient occurs.
(a) Condition on slow cooling and at equilibrium with the liquid bath. (b) Condition during heating. The segment of the link which has no gradient in marked as B since it is at the same temperature as the bath.

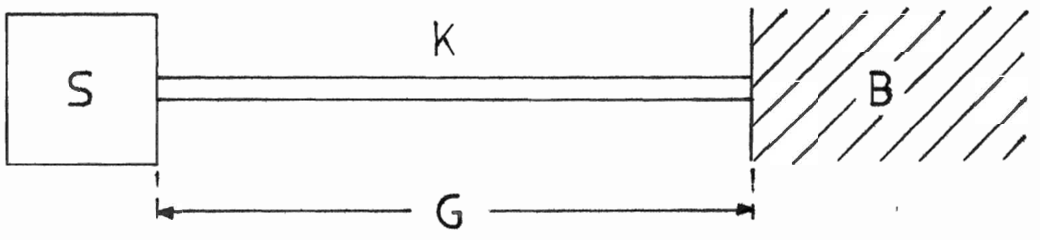

(a)

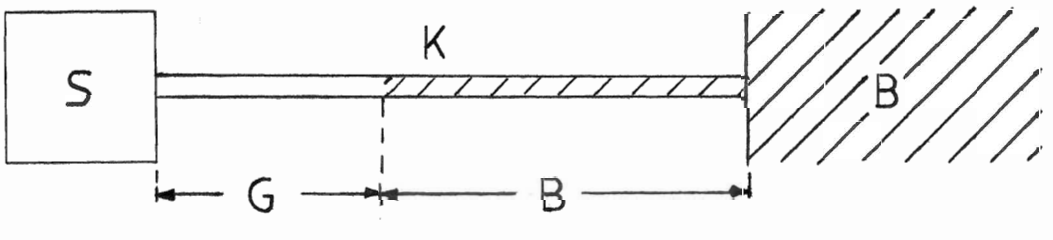

(b)

Figure IV.1

Several change were made to the calorimeter as described in section I. The wires running from the connector were all changed using manganin wire and 50 gauge copper wire for the electrical connections. Short copper posts were epoxied into the bass plate of the copper bath (ie. plate below bath heater). These provided well thermalized electric pass-throughs to the sample region. A much less massive shield was made from a rolled copper sheet. The sample mount sheet was cut nearly in half (approx. 30 mg) and a new larger sample (0.594 g) was used.

The analysis has also been changed. Instead of using the divided differences derivative calculation, the data is fitted in sections to a third degree polynomial using the least squares method provided by Lotus 123. Similarly the P(T) data is fitted to second degree polynomial. This approach of course gives a smooth curve.

Decay times are now on the order of 700 sec for a decay from approximately 27K to 6K. Analysis has provided good results consistently. Figures IV.2 to IV.4 show the results of a typical experiment. Figures IV.2 and IV.3 show P(T) and the decay respectively, both are smooth and well behaved. The heat capacity as a function of time is provided in figure IV.4. The lower curve shows the accepted data for a sample / mount sheet combined mass of 0.624 g. There is a discrepancy between the data, addenda appears temperature dependent as expected for the heat capacity of the strain gauge, thermometer and GE varnish.

To verify that the discrepancy is due to the remaining heat capacities, a second experiment without the sample must be performed. However at this time this data is not yet available but the experiment will be performed in the near future. However it is believed that this method has been successfully implemented.

Figures IV.2 -IV.4

Figure IV.2, Power vs Temperature

Graph of heater power as a function of temperature. Experimental data is fitted to a second degree polynomial.

Figure IV.3, Temporal Response on Decay

Graph of sample temperature as a function time on decay. Data fitted to a third degree polynomial.

Figure IV.4, Heat Capacity

Upper graph shows total heat capacity as a function of temperature from experimental data. Lower graph gives accepted data for a mass of 0.624g.

Figure IV.2

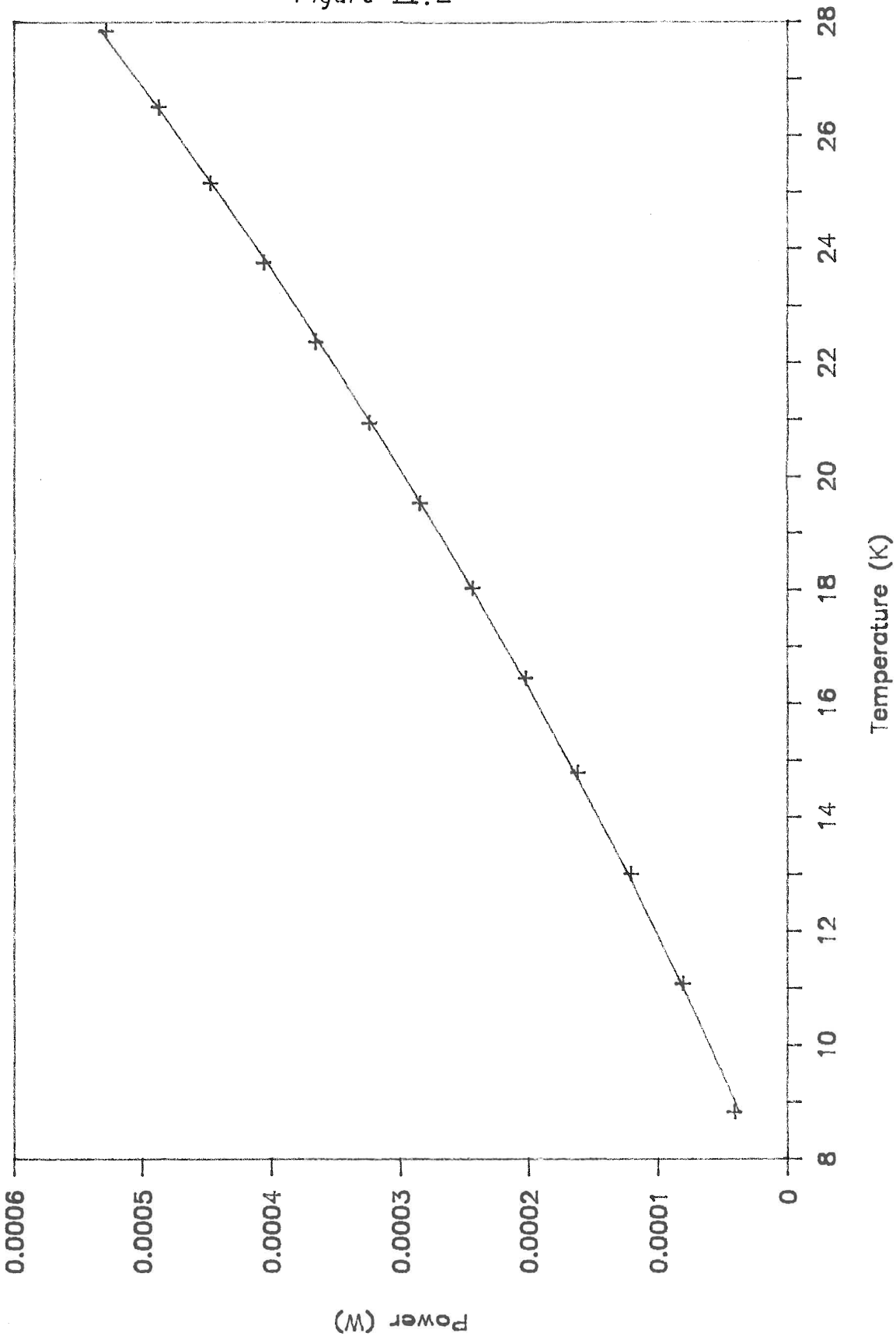
Power (W)
0.0006
0.0005
0.0004
0.0003
0.0002
0.0001
0
8
10
12
14
16
18
20
22
24
26
28
Temperature (K)

Figure IV.3

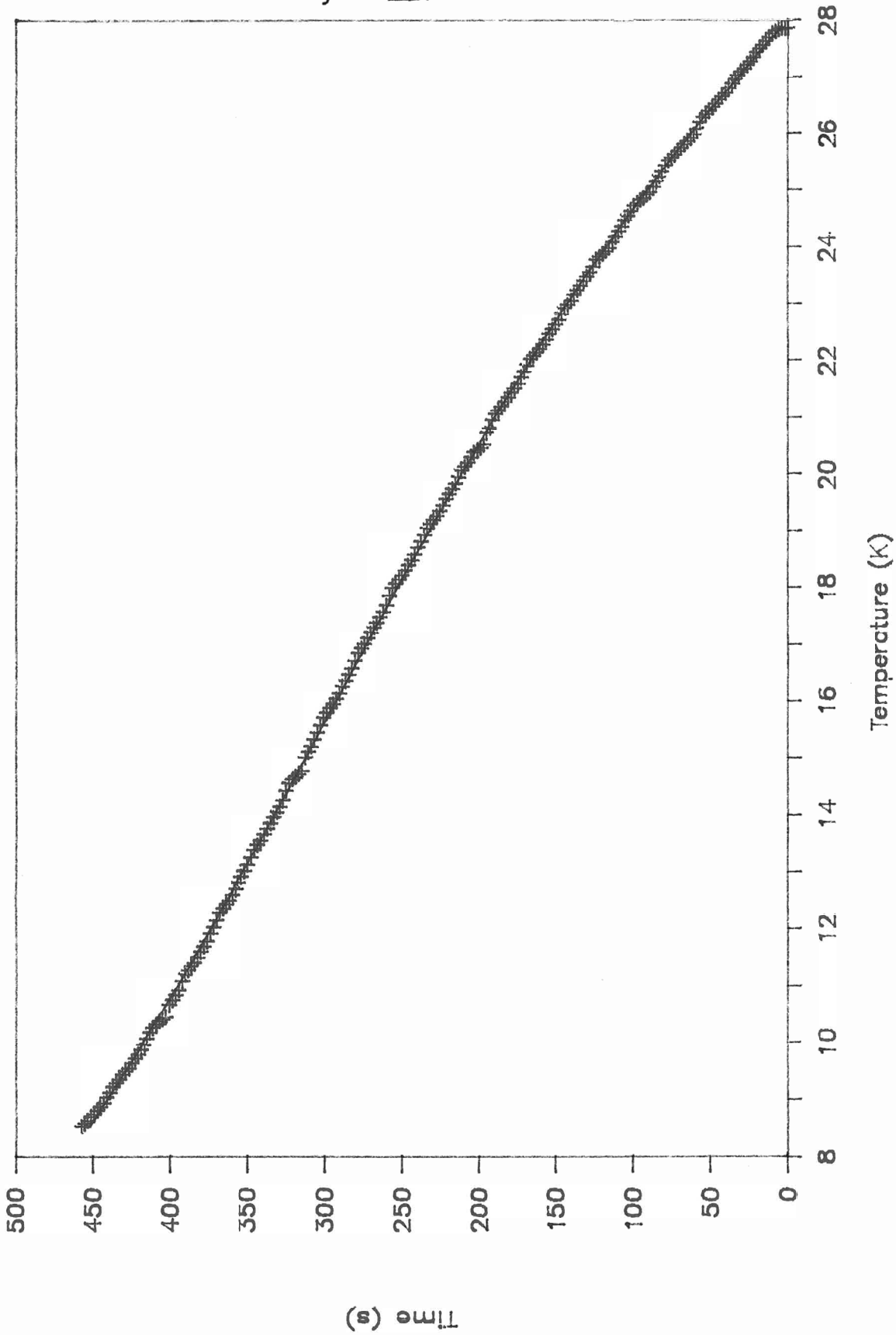
Temperature (K)
8
10
12
14
16
18
20
22
24
26
28
Time (s)
0
50
100
150
200
250
300
350
400
450
500

Figure IV.4

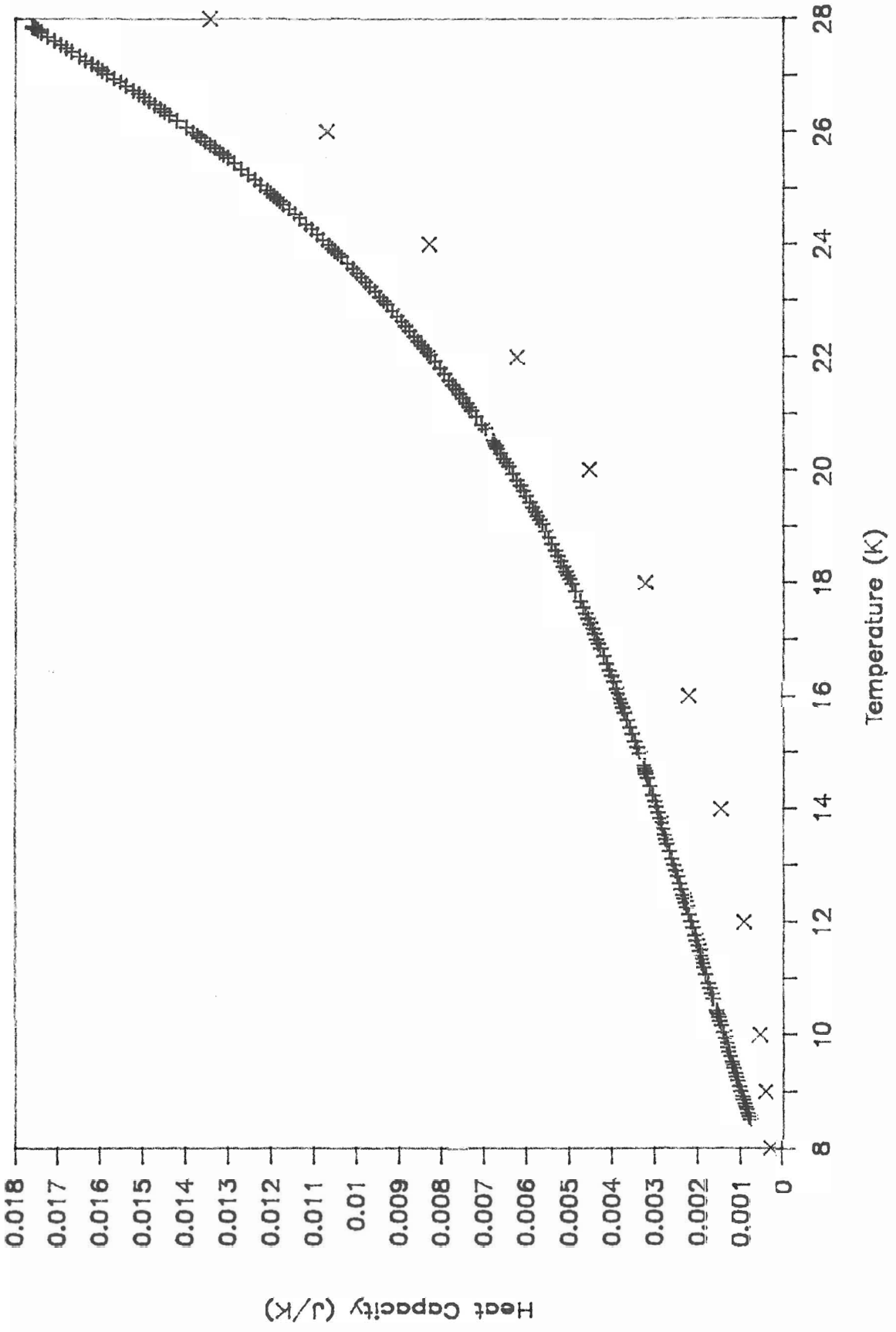
Heat Capacity (J/K)
0.018
0.017
0.016
0.015
0.014
0.013
0.012
0.011
0.01
0.009
0.008
0.007
0.006
0.005
0.004
0.003
0.002
0.001
0
8
10
12
14
16
18
20
22
24
26
28
Temperature (K)

Summary and Concluding Remarks

In all three methods of measuring heat capacity were investigated and separately reported on in sections II, III and IV. These systems were chosen and designed to meet two criteria; they should be able to measure small samples and capable of a fully automated operation over the temperature range of 15-300K.

The modified heat step method of section II proved unacceptable in that the measured heat capacity showed a high degree of scatter. It was believed that the reason for the failure of this method is the existence of an unavoidable upward drift in temperature which had a critical effect on the calculation of the heat capacity. The only way to reduce this drift is to use an adiabatic calorimeter which is inconsistent with the method. The automation and program design of this method were successful and were capable of operating over the desired temperature range.

The continuous heating method as implemented in section III has provided favourable results with smooth, well behaved data obtained for all aspects of the measurement. However at this time only measurements of the so called pseudo heat capacity are available and further investigation is required to establish the full success of this implementation. It is also believed that the system can be further improved by modifying some aspects of the temperature control methods used presently.

The decay method of section IV has been the most successful of

the three methods. The data obtained for all aspects of the experiments were smooth, well-behaved and well-resolved. The experimental data for heat capacity proved reproducible and appears to be in good agreement with the accepted data for copper.

All three methods were successful in achieving an automated system, but the two final methods must be used together to cover the desired temperature range since the decay method is useful below 40K and the continuous heating method is applicable above 40K. However the thermal characteristics (specifically the thermal link between the sample and its environment) of the calorimeter are not compatible for the two methods. Therefore practical use will require that a second calorimeter be built. As a final note it was found in general that analog PID (Proportional, Integral, Derivative) temperature control is most effective.

References

1. J. M. DePuydt and E. D. Dahlberg, Low Temperature Calorimetry for Small Samples, Rev. Sci. Inst., v57(3), 1986, p483-6.

2. A. Junod, Automated Calorimeter for Temperature Range 80-230K Without Use of a Computer, J. Phys. E, Sci. Inst., v12, 1979, p945-52.

3. R. Bachmann et al, Heat Capacity Measurements on Small Samples at Low Temperatures, Rev. Sci. Inst., v43(2), 1972, p205-213.

4. Cryo Industries of America, General Manual and Catalog for their Cryostats (available in the lab).

5. Scientific Instruments, Series 5500 Temperature Controller Manual, (available in the lab).

6. Scientific Solutions, IEEE Interface User and Reference Manual, (available in the lab).

7. Prema Integrating Scanner User Manual, (available in the lab).

8. Lakeshore Cryogenics, DRC-91C Temperature Controller Manual, (available in the lab).

9. F. G. Curtis and P. O. Wheatly, Applied Numerical Analysis, 3rd edition, p191-6.

10. W. N. Lawless, C. E. Clark and R. W. Arenz, Method for Measuring Specific Heats in Intense Magnetic Fields at Low Temperatures Using Capacitance Thermometry, Rev. Sci. Inst., v53(11), 1982, p1647-52.

11. G. R. Stewart, Measurement of Low-temperature Specific Heat, Rev. Sci. Inst., v54(1), 1983, p1-11.

12. R. B. Rogge, Supplement to Study of Heat Capacity Measurement Methods, (1990), (available from Dr. F. S. Razavi, department of Physics); Note: the letter following reference indicates the relevant appendix of the supplement.

13. E. S. R. Gopal, Specific Heats at Low Temperatures, (1966), p7-10.

Additional useful references not explicitly referenced in this report.

G. K. White, Experimental Techniques in Experimental Physics, (1968)

G. R. Stewart, Measurement of Low-temperature Specific Heat, Rev. Sci. Instrum. 54(1), (1983), p1-11. (Review Article)

H. E. Fischer, S. K. Watson and D. G. Cahill, Specific Heat, Thermal Conductivity and Electrical Resistivity of High Temperature Superconductors, Comments on Cond. Mat. Phys., 14(2), p65-127.